The Thesis committee for Kyle Brady Hollingshead
Certifies that this is the approved version of the following thesis:

Efficient Computational Strategies for Predicting Homogeneous Fluid Structure

APPROVED BY

SUPERVISING COMMITTEE:

Thomas M. Truskett, Supervisor

Venkat Ganesan

Efficient Computational Strategies for Predicting Homogeneous Fluid Structure

by

Kyle Brady Hollingshead, B.S.C.E.

THESIS

Presented to the Faculty of the Graduate School of

The University of Texas at Austin

in Partial Fulfillment

of the Requirements

for the Degree of

MASTER OF SCIENCE IN ENGINEERING

THE UNIVERSITY OF TEXAS AT AUSTIN

August 2014

For Fran

Acknowledgments

First and foremost I must thank Tom Truskett for the past five years of encouragement, patience, insight, and advice. He has helped me grow into a stronger researcher and a better person.

I am also thankful for all of the people I've had the fortune to share a laboratory with. Mark Pond and James Carmer were great role models and kept the lab lively and cheerful. Avni Jain has been a bright source of positive energy and optimism, and a wonderful and talented collaborator; it's been a pleasure moving through graduate school side by side. Jonathan Bollinger brought renewed intellectual vigor and passion for inquiry to the lab, and inspires everyone around him to greater achievements. I worked with Theodore "Tres" Popp only briefly, and hope he has not been corrupted too thoroughly. I am proud to count all of them among my friends.

If not for Paul Blowers, I would have never known the giddy satisfaction that comes from solving a research problem after long struggle, and likely would not have pursued a graduate degree. I owe him a debt for his willingness to take a chance on a second-semester freshman, and for all of the wisdom and guidance he has shared since.

I am grateful that Matt West's only graduate school option was to join me in Austin as he did in Tucson. He has been a rock of stability over the

past decade: no matter how hectic, stressful, or chaotic life might have been, I could always count on a friend with whom I could have lunch.

While it likely goes without saying, permit me to say anyway that none of my successes would have been possible without the tireless support of my parents, Kevin and Susan, and my sister Alexis. Thanks to them, I can reach higher and stretch further, knowing that if I fall, someone is always there to catch me.

And finally, I thank my wife Fran Gaede for her endless love and support. She makes the worst days bearable and the best days exquisite, and every day I am overjoyed that she is a part of my life.

Efficient Computational Strategies for Predicting Homogeneous Fluid Structure

Kyle Brady Hollingshead, M.S.E.
The University of Texas at Austin, 2014

Supervisor: Thomas M. Truskett

A common challenge in materials science is the "inverse design problem," wherein one seeks to use theoretical models to discover the microscopic characteristics (e.g., interparticle interactions) of a system which, if fabricated or synthesized, would yield a targeted material property. Inverse design problems are commonly addressed by stochastic optimization strategies like simulated annealing. Such approaches have the advantage of being general and easy to apply, and they can be effective as long as material properties required for evaluating the objective function of the optimization are feasible to accurately compute for thousands to millions of different trial interactions.

This requirement typically means that "exact" yet computationally intensive methods for property predictions (e.g., molecular simulations) are impractical for use within such calculations. Approximate theories with analytical or simple numerical solutions are attractive alternatives, provided that they can make sufficiently accurate predictions for a wide range of microscopic interaction types.

We propose a new approach, based on the fine discretization (i.e., terracing) of continuous pair interactions, that allows first-order mean-spherical approximation theory to predict the equilibrium structure and thermodynamics of a wide class of complex fluid pair interactions. We use this approach to predict the radial distribution functions and potential energies for systems with screened electrostatic repulsions, solute-mediated depletion interactions, and ramp-shaped repulsions.

We create a web applet for introductory statistical mechanics courses using this approach to quickly estimate the equilibrium structure and thermodynamics of a fluid from its pair interaction. We use the applet to illustrate two fundamental fluid phenomena: the transition from ideal gas-like behavior to correlated-liquid behavior with increasing density in a system of hard spheres, and the water-like tradeoff between dominant length scales with changing temperature in a system with ramp-shaped repulsions.

Finally, we test the accuracy of our approach and several other integral equation theories by comparing their predictions to simulated data for a series of different pair interactions. We introduce a simple cumulative structural error metric to quantify the comparison to simulation, and find that according to this metric, the reference hypernetted chain closure with a semi-empirical bridge function is the most accurate of the tested approximations.

Table of Contents

List of Tables

List of Figures

Chapter 1

Introduction

Effective interactions between suspended colloids or nanoparticles can be experimentally tuned (e.g., by changing the properties of the solvent, through physical or chemical modification of the particles, or via external fields) so that macroscopic properties of the corresponding complex fluids can be engineered from the "bottom up" [17, 27, 46, 72]. Statistical mechanics provides a formal quantitative framework that links microscopic properties to macroscopic behavior, in principle allowing for computational inverse design of interparticle interactions to achieve desired material characteristics (*e.g.,* specific structural features or other targeted properties via structure-property relations) [7, 14, 20, 23, 25, 26, 29, 40, 41, 63, 67].

In practice, successful inverse design strategies rely upon on accurate and efficient means for solving a forward version of the problem at hand. Molecular simulations or sophisticated integral equation theories–otherwise well suited for the forward calculation of equilibrium behavior from microscopic interactions–currently require computational resources that are prohibitive for use in most optimization strategies. Simple analytic liquid-state theories are a potentially attractive alternative, but they are unfortunately limited in terms

of the types of pair potentials that they can accurately treat [31].

In Chapter 2, we develop a simple and general analytical strategy for predicting the equilibrium structure and thermodynamics of complex fluids by terracing continuous pair interactions in order to apply first-order mean-spherical approximation theory. Specifically, we implement a version of this approach to predict how screened electrostatic repulsions, solute-mediated depletion attractions, or ramp-shaped repulsions modify the radial distribution function and the potential energy of reference hard-sphere fluids, and we compare the predictions to exact results from molecular simulations.

In Chapter 3 we present a web applet designed for classroom use or as a guide to experiment, which uses the discretization strategy described in Chapter 2 to quickly and semi-quantitatively estimate the equilibrium radial distribution function and related thermodynamic properties of a fluid from knowledge of its pair interaction. We present a detailed description of the applet's features and intended workflow, followed by a description of how the applet can be used to illustrate two (of many possible) concepts of interest for introductory statistical mechanics courses: the transition from ideal gas-like behavior to correlated-liquid behavior with increasing density and the tradeoff between dominant length scales with changing temperature in a system with ramp-shaped repulsions. The latter type of interaction qualitatively captures distinctive thermodynamic properties of liquid water because its energetic bias toward locally open structures mimics that of water's hydrogen-bond network.

Since finely terraced potentials can accurately represent their continu-

ous counterparts, in Chapter 4 we assess the utility of several integral equation theories for predicting the structure of fluids with pair interactions of this type. We use molecular dynamics simulations to test the accuracy of fluid structure predictions made using simple and computationally efficient closures (including Percus-Yevick, hypernetted chain, reference hypernetted chain with an analytical bridge function, first-order mean spherical approximation, and a modified first-order mean spherical approximation,) for eight different piecewise-constant pair interactions comprising a hard core and a combination of two shoulders and/or wells. To quantify the comparison to simulation, we introduce a simple cumulative structural error metric which qualitatively predicts thermodynamic accuracy. For equilibrium fluid state points of these models, we find that the reference hypernetted chain closure is the most accurate of the tested approximations as characterized by this metric.

Chapter 2

Fine discretization of pair interactions and an approximate analytical strategy for predicting equilibrium behavior of complex fluids

In this chapter, we explore whether fine discretization (i.e., terracing) of the pair interaction can allow one to use analytical theories in a new way to predict the behaviors of a broader range of model complex fluids, rendering these analytical methods more powerful as tools for materials design. In other contexts, theoretical studies have characterized the thermodynamics of terraced potentials comprising a limited number of square wells or shoulders [11, 37, 62]. Fine discretization of continuous pair interactions has also been utilized in order to take advantage of efficient event-driven simulation algorithms [10, 70].

Our proposed strategy comprises three parts: (1) fine discretization of a short-range, continuous pair potential into a terraced representation, (2) application of an approximate, analytical liquid-state theory capable of accu-

This chapter first appeared as "Kyle B. Hollingshead, Avni Jain, and Thomas M. Truskett. Communication: Fine discretization of pair interactions and an approximate analytical strategy for predicting equilibrium behavior of complex fluids. *The Journal of Chemical Physics,* 139(16):161102, 2014." Avni Jain performed Monte Carlo simulations, and Thomas Truskett supervised the work.

rately predicting the finely sawtoothed radial distribution function (RDF) of the terraced model, and (3) smoothing of the sawtoothed RDF to recover a continuous prediction for the pair correlation function of the fluid with the original potential.

To test the performance of this discretization-and-smoothing based approach, we compare its predictions to exact (within numerical precision) results from molecular simulations. Specifically, we study the accuracy of its predictions for how short-range screened electrostatic (Yukawa) [19, 21, 33] repulsions, solute-induced depletion (Asakura-Oosawa) [8, 58] attractions, or ramp-shaped [24, 39, 71] repulsions modify the equilibrium structure and thermodynamics of a hard-sphere fluid.

2.1 Methods

2.1.1 Discretization Strategy

We consider isotropic, pairwise interparticle interactions $\varphi(r)$ that consist of a hard-core exclusion for separations less than a particle diameter ($r < \sigma$) plus a continuous, short-range contribution $\phi(r)$ that decays to zero by a cut-off r_c,

$$\varphi(r) = \begin{cases} \infty & r < \sigma \\ \phi(r) & \sigma \leq r < r_c \\ 0 & r \geq r_c \end{cases} . \tag{2.1}$$

We discretize the continuous potential into a terraced representation of M steps, each with a constant energy

$$\varepsilon_i = (\lambda_i - \lambda_{i-1})^{-1} \int_{\lambda_{i-1}}^{\lambda_i} \phi(r)\, dr, \tag{2.2}$$

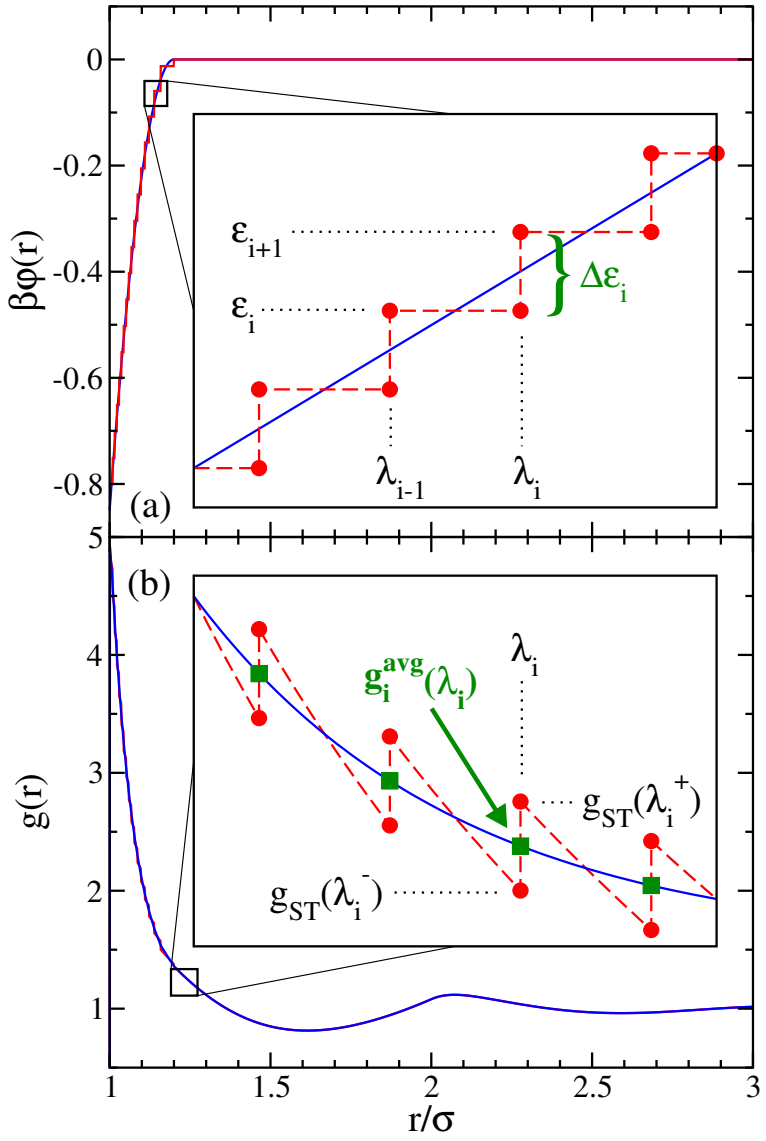

Figure 2.1: Schematic of potential terracing and RDF smoothing. (a) The continuous potential of interest $\beta\varphi(r)$ (blue, solid) and the corresponding terraced version (red, dashed) are shown, with parameters ϵ_i and λ_i determined from Eq. 2.2 as described in the text. (b) The sawtoothed RDF $g_{\mathrm{ST}}(r)$ (red, dashed) associated with the terraced potential is computed using Eq. 2.3. It is smoothed using Eqs. 2.4 and 2.5 to arrive at a continuous prediction (blue, solid) for the RDF of the fluid with the original potential.

where λ_i is the outer boundary of step i (see Figure 2.1a). The values of ε_i and λ_i are determined simultaneously, beginning from r_c and working inward, such that the difference in energies between neighboring steps, $\Delta\varepsilon_i = \varepsilon_{i+1} - \varepsilon_i$, is smaller in magnitude than a specified threshold $\Delta\varepsilon^{max}$. This threshold should be small enough that the terraced representation adequately captures the shape of the continuous potential. In this work, we set $\beta\Delta\varepsilon^{max} = 0.05$, where $\beta = (k_\mathrm{B}T)^{-1}$, k_B is the Boltzmann constant and T is temperature. A more extensive discussion how our strategy depends on this parameter is available in Appendix A.

Terraced potentials produce sawtoothed shaped RDFs, $g_\mathrm{ST}(r)$, which we compute here via an extension of the simple exponential first-order mean spherical approximation (SEXP-FMSA) proposed by Hlushak, et al. for square-shoulder systems [36], which itself is a variation of the first-order mean spherical approximation (FMSA) of Tang and Lu [64, 65]. We treat each step in the discretized potential as an independent perturbation[1] to the RDF of the reference hard-sphere fluid at the same packing fraction η:

$$g_\mathrm{ST}(r) = g_\mathrm{HS}(r) \prod_{i=1}^{M} \exp\left[-\beta\Delta\varepsilon_i g_\mathrm{FMSA}(r, \lambda_i, \eta)\right] \tag{2.3}$$

where $g_\mathrm{HS}(r)$ is the RDF of the hard-sphere fluid, and $g_\mathrm{FMSA}(r, \lambda_i, \eta)$ is the FMSA perturbation defined by Eq. 73 of Ref. [65]. The quantity $g_\mathrm{FMSA}(r, \lambda_i, \eta)$ depends on λ_i and $\eta = \pi\rho\sigma^3/6$, where ρ is the number density. This particular

[1]This type of approximation is natural for approaches which, like FMSA, assume a linear dependence of the RDF on the interaction energy.

approximation is capable of treating terraced potentials with a cut-off $r_c \leq 2\sigma$, a constraint that might be relaxed in future implementations by choosing a different analytical theory for this step.

To arrive at a continuous prediction for the pair correlations of the fluid with the original potential, we smooth out the "teeth" in $g_{\mathrm{ST}}(r)$ by adding a correction $\Delta g\,(r)$,

$$g\,(r) \equiv g_{\mathrm{ST}}\,(r) + \Delta g\,(r)\,, \tag{2.4}$$

which is a piecewise sequence of linear functions:

$$\begin{aligned} \Delta g\,(r) \equiv \quad & \left[g_i^{avg} - g_{\mathrm{ST}}\left(\lambda_i^-\right)\right]\left(\frac{r-\lambda_{i-1}}{\lambda_i-\lambda_{i-1}}\right) \\ & + \left[g_{i-1}^{avg} - g_{\mathrm{ST}}\left(\lambda_{i-1}^+\right)\right]\left(1-\frac{r-\lambda_{i-1}}{\lambda_i-\lambda_{i-1}}\right) \\ & \text{for} \quad \lambda_{i-1} < r < \lambda_i, \end{aligned} \tag{2.5}$$

with $g_i^{avg} = \left[g_{\mathrm{ST}}\left(\lambda_i^-\right) + g_{\mathrm{ST}}\left(\lambda_i^+\right)\right]/2$.

2.1.2 Model Pair Interactions

As alluded to above, we consider three forms for $\phi(r)$ in Eq. 2.1: screened electrostatic (Yukawa) [19, 21, 33] repulsions, solute-induced depletion (Asakura-Oosawa) [8, 58] attractions, or ramp-shaped [24, 39, 71] repulsions.

Screened electrostatic repulsions. The repulsive Yukawa potential can be expressed as

$$\phi_{\mathrm{Y}}\,(x) = \gamma x^{-1} \exp\left[-\kappa\,(x-1)\right], \tag{2.6}$$

where $x = r/\sigma$, $\gamma > 0$ is the energy at contact (effective Yukawa charge), and κ^{-1} is the screening length. To avoid discontinuities, we adopt a form that is cut at $x_c = 2$ and shifted

$$\phi(x) = \phi_{\mathrm{Y}}(x) - \phi_{\mathrm{Y}}(x_c). \tag{2.7}$$

Depletion attractions. The Asakura-Oosawa (AO) model for non-interacting, solute-induced depletion attractions can be expressed

$$\beta\phi(x) = -\frac{\eta_p}{(1 - x_c^{-1})^3}\left[1 - \frac{3}{2}\frac{x}{x_c} + \frac{1}{2}\left(\frac{x}{x_c}\right)^3\right] \tag{2.8}$$

for $1 \leq x \leq x_c$ and $x_c = (1 + q)$. Here, q is the implicit solute to explicit particle diameter ratio, and η_p is the packing fraction of implicit solute particles.

Ramp-shaped repulsions. In its simplest form, the hard-core plus repulsive ramp potential is:

$$\phi(x) = U_1[1 - (x/x_c)] \tag{2.9}$$

for $1 \leq x \leq x_c$. Here, U_1 is the characteristic energy scale of the ramp, and we choose $x_c = 2$.

2.1.3 Molecular Simulations

We test the discretization-and-smoothing strategy by comparing its smoothed RDF and potential energy predictions with exact results from canonical-ensemble Monte Carlo molecular simulations. We initialized the Monte Carlo

simulations with either $N = 2744$ particles (for systems with Yukawa repulsions) or $N = 1000$ particles (for systems with AO depletion attractions or ramp-shaped repulsions) in disordered configurations within a cubic simulation box, using periodic boundary conditions. After an initial equilibration period at the temperature of interest, we collected properties over a period of 10^6 Monte Carlo cycles.

2.2 Comparison of Analytical Predictions to Simulation Results

To assess the performance of our proposed theoretical strategy, we investigate its ability to predict static structure (quantified by the RDF) and potential energy for the three model systems discussed above.

The predicted RDFs of Eq. 2.4 and those computed from simulations for a range of packing fractions ($\eta = 0.25$–0.45) and potential interaction strengths are presented in Figure 2.2. Broadly speaking, the predictions capture the simulated pair correlations of the three systems, despite the fact that each represent significant–and qualitatively different–departures from the structure of the hard-sphere fluid. The theoretical strategy predicts the most accurate structures for higher packing fractions and weaker interactions. The only qualitative failing appears in the strongly interacting repulsive-ramp fluid at low density, where the contact value of the RDF is significantly underpredicted.

Potential energies predicted by our strategy and those computed from simulations as functions of interaction strength and packing fraction are pre-

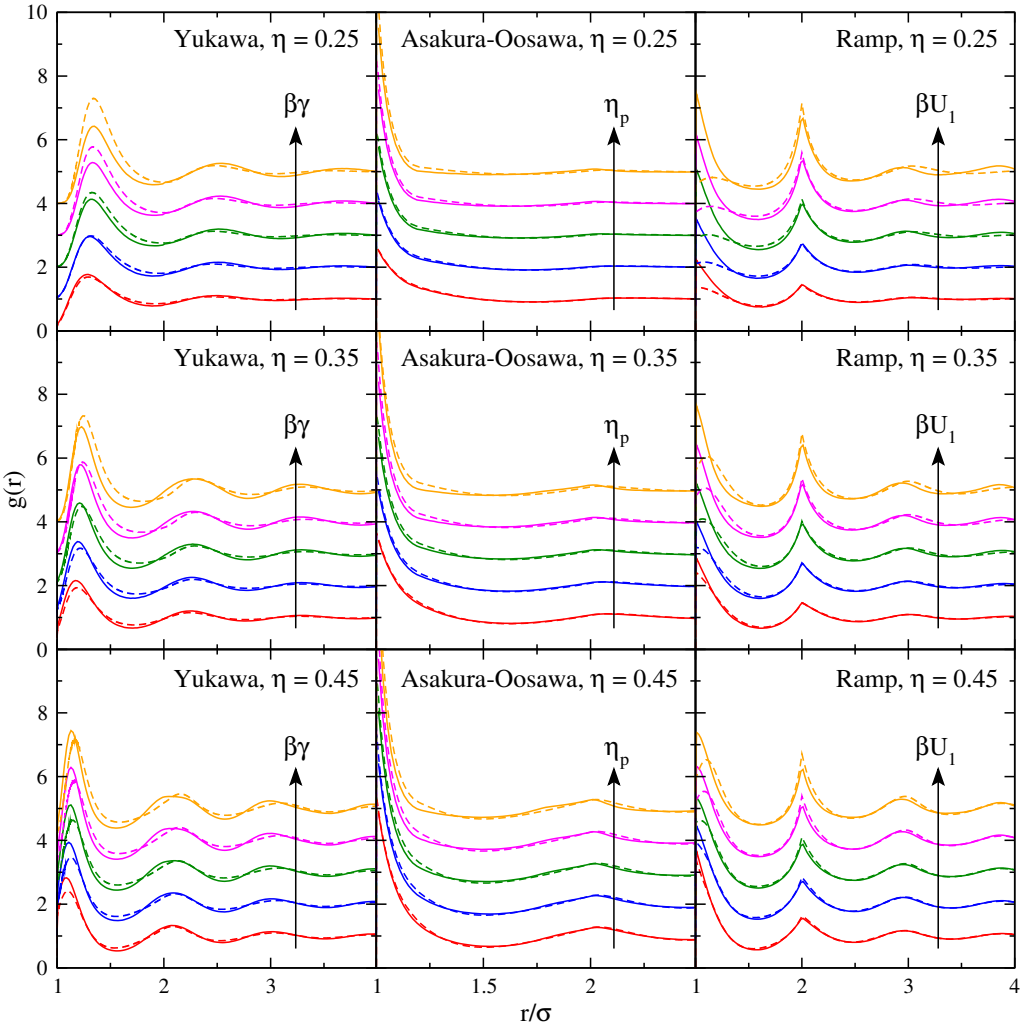

Figure 2.2: RDFs of fluids with particles interacting via hard-sphere plus Yukawa repulsions, Asakura-Oosawa (AO) depletion attractions, and ramp-shaped repulsions at packing fractions $\eta = 0.25$, 0.35, and 0.45. Shown are predictions of Eq. (2.4) (dashed lines) and results of Monte Carlo simulations (solid lines). For the Yukawa repulsions, $\kappa = 5$ and $\beta\gamma = 5$ (red), 7.5 (blue), 10 (green), 12.5 (magenta), or 15 (orange). For the AO depletion attraction, $q = 0.2$ and $\eta_p = 0.04$ (red), 0.08 (blue), 0.12 (green), 0.16 (magenta), or 0.2 (orange). For the repulsive ramp interaction, $r_c = 2\sigma$ and $\beta U_1 = 10$ (red), 15 (blue), 20 (green), 25 (magenta), or 30 (orange). Curves for different interaction strengths are shifted vertically by integer values for clarity.

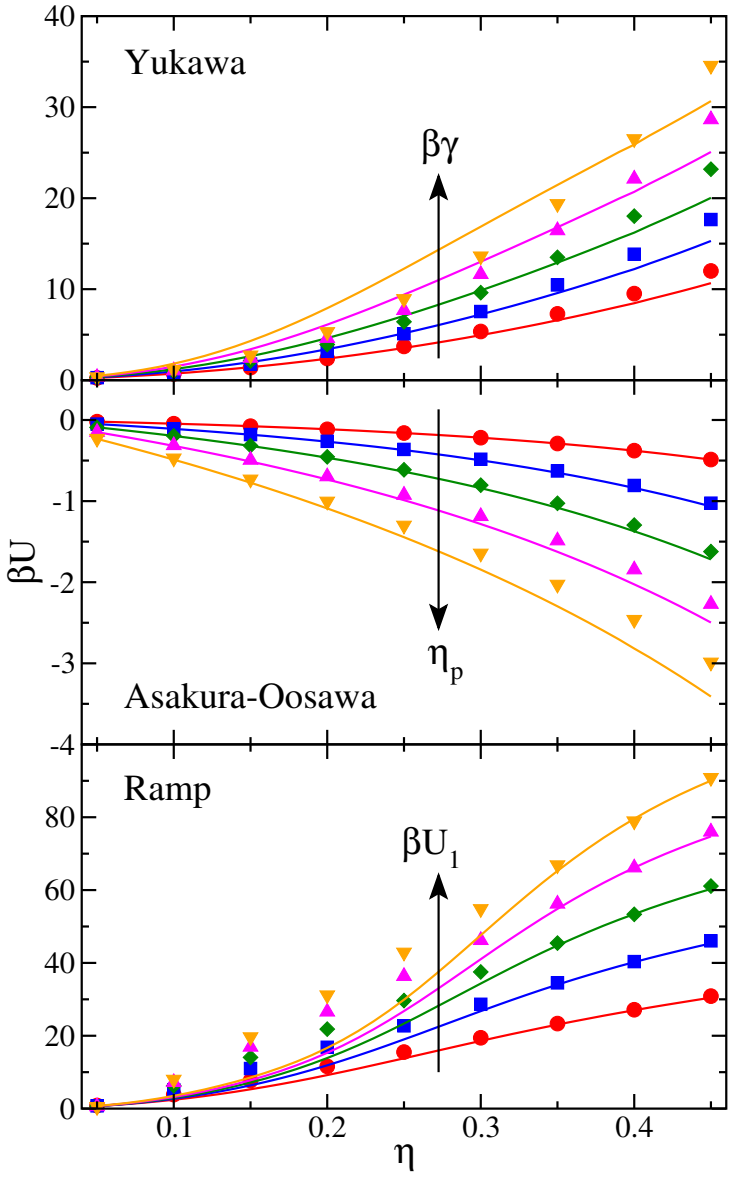

Figure 2.3: Potential energy βU versus packing fraction η for fluids with particles interacting via hard-sphere plus Yukawa repulsions, Asakura-Oosawa (AO) depletion attractions, and ramp-shaped repulsions. Solid curves are obtained from the predicted RDFs via $\beta U = (\beta/2) \int \varphi(r) g(r) d\mathbf{r}$, and symbols are results from Monte Carlo simulations. Interaction potential parameters for each system ($\beta\gamma$, ϕ_p, and βU_1) are the same as in Fig. 2.2.

sented in Figure 2.3. In general, the trends track what might be expected from the RDFs shown in Figure 2.2: very good agreement at high packing fractions, except at the highest potential interaction strengths, and also good agreement for low interaction strengths at all packing fractions (especially for the fluid with AO depletion attractions). The largest quantitative deviations of the theoretical predictions from the simulations occur for repulsive Yukawa fluid and the repulsive ramp model for strong energies of interaction in the packing fraction range ($\eta < 0.25$).

2.3 Conclusion

In summary, the analytical, discretization-based approach we introduce here can predict the thermodynamic and structural consequences of some of the diverse types of short-range interactions that naturally emerge in dense, complex fluids (e.g., suspended colloids). Since good predictive strategies can provide guidance on how best to tune these systems to achieve desired changes in macroscopic properties, this approach represents a promising new strategy for using analytical liquid-state perturbation theories as tools for materials design.

Chapter 3

A web-applet for rapidly predicting fluid structure and thermodynamics

Statistical mechanics provides quantitative links between a fluid's interparticle interactions and its resulting equilibrium structure and thermodynamic properties. However, particularly for dense systems or systems with complex interactions, it can be challenging to find ways for students to explore these relationships within the framework of a university course due to the prohibitive amount of time, expertise (either computational or experimental), and/or resources required to, e.g., numerically solve the Ornstein-Zernike relation with an appropriate closure [31, 65], construct a molecular simulation to extract relevant equilibrium data [5, 49, 53], or carry out relevant measurements in a laboratory [33, 73]. As a result, for students to become familiar with the relevant concepts, additional tools are required that help them to overcome these technical hurdles.

Here, we present a web-based applet that helps to accomplish this through use of the analytic integral equation-based method for equilibrium fluids in three dimensions described in Chapter 2. The applet provides rapid and semi-quantitative graphical predictions of structural and thermodynamic

quantities from knowledge of the pair interaction and parameters that describe the thermodynamic state (i.e., density and temperature). Apart from awareness of a few practical constraints, detailed knowledge of the internal calculations is not required to make productive use of the applet as a pedagogical tool or as an experimental guide. Because of its efficiency and accessible layout, students are empowered to interactively experiment with a fluid's pair potential or its thermodynamic state and extract meaningful relationships and trends [13, 16, 45, 66, 69].

3.1 Internal Calculations

The applet accepts as inputs a pairwise potential $\varphi(r)$ as a function of interparticle separation r, the temperature T, and the number density ρ, and it approximately calculates the corresponding unique radial distribution function (RDF) [35] as well as other related thermodynamic quantities. The applet requires that the interactions be isotropic, consisting of a hard core of diameter σ plus an arbitrary short-ranged contribution $\varepsilon\phi(r)$, where ε is a characteristic energy scale, that decays to zero by $r = 2\sigma$,

$$\frac{\varphi(r)}{\varepsilon} = \begin{cases} \infty & r < \sigma, \\ \phi(r) & \sigma \leq r \leq 2\sigma, \\ 0 & r > 2\sigma. \end{cases} \tag{3.1}$$

As we showed in Chapter 2, by choosing different functions for $\phi(r)$, this generic form encompasses many different types of effective model interactions routinely used to describe the thermodynamics and structure of complex fluids. Two possible choices–a bare hard-sphere potential, for which $\phi(r) = 0$,

that models excluded-volume interactions in fluids and a repulsive ramp potential, for which $\phi(r) = 2 - r/\sigma$, that qualitatively captures some distinctive properties of liquid water–are discussed explicitly in this chapter. Other possible model interactions include, but are not limited to, Yukawa potentials that model screened electrostatic interactions in colloidal suspensions and dusty plasmas [19, 21, 33] and the Asakura-Oosawa potential [8, 58] that models polymer-mediated depletion interactions between suspended colloids.

3.1.1 Radial Distribution Function

To enable the desired predictions, the applet first decomposes the continuous potential interaction into a "terraced" representation of $M = 100$ equally-spaced discrete steps, each with an outer range

$$\frac{\lambda_i}{\sigma} = 1 + \frac{i}{M} \tag{3.2}$$

and a constant energy

$$\frac{\varphi_i}{\varepsilon} = (\lambda_i - \lambda_{i-1})^{-1} \int_{\lambda_{i-1}}^{\lambda_i} \phi(r)\, dr. \tag{3.3}$$

The integration in Eq. (3.3), and other integrations for the applet are carried out via the trapezoidal rule.

A terraced potential yields a jagged or "sawtoothed" RDF, $g_{\mathrm{ST}}(r)$, which is computed via the extension of the simple exponential first-order mean spherical approximation [36] described in Chapter 2. Then, to arrive at a continuous RDF prediction that corresponds to the original continuous potential,

the "teeth" are smoothed by computing a series of linear corrections to $g_{\mathrm{ST}}(r)$ such that adjacent pieces of the smoothed RDF, $g(r)$, have equal values at each intersection, i.e. $g(\lambda_i^-) = g(\lambda_i^+)$, where the superscripts $^-$ or $^+$ indicate limiting values approaching each λ_i from the left or right, respectively. (See Chapter 2 for details).

3.1.2 Thermodynamic Properties

The applet calculates several thermodynamic properties that are directly accessible via the pair potential and the RDF. The internal energy per particle u is [31]

$$u = \frac{3k_{\mathrm{B}}T}{2} + 2\pi\rho \int_0^\infty \varphi(r)\, g(r) r^2\, dr, \tag{3.4}$$

where k_{B} is the Boltzmann constant, T is temperature, $\rho = N/V$, N is total number of particles, and V is volume. The compressibility factor Z is [9]

$$Z = \frac{\beta P}{\rho} = 1 + \frac{2\pi\rho}{3} \sum_{i=0}^{M} {\lambda_i}^3 \left[g_{\mathrm{ST}}(\lambda_i^+) - g_{\mathrm{ST}}(\lambda_i^-) \right], \tag{3.5}$$

where $\beta = (k_{\mathrm{B}}T)^{-1}$, P is the pressure, and λ_i is given by Eq. (3.2). Note that the excess Helmholtz free energy of the fluid (and other properties of interest through standard thermodynamics relations) can subsequently be obtained from knowledge of the density and temperature dependence of Z, i.e., the equation of state [31]. The two-body contribution to molar excess entropy $s^{(2)}$ is also directly computable from the RDF [14, 42, 52],

$$\frac{s^{(2)}}{k_{\mathrm{B}}} = -2\pi\rho \int_0^\infty \left[g(r) \ln g(r) - g(r) + 1 \right] r^2\, dr. \tag{3.6}$$

This last quantity–the entropy cost of pair correlations (relative to a structure-free ideal gas)–is of interest because it is known to correlate with dynamic properties (e.g., self diffusivity) in a wide class of fluid systems [14, 22, 42, 52, 56, 57].

3.2 Using the Applet

The applet is written in Java using the Swing library,[1] which ensures portability across different operating systems and allows the applet to be embedded in a web page. Graphs are created with the JFreeChart library[2] to allow for easy visualization, manipulation, and analysis of series data. A system–comprising the pair potential, the thermodynamic state ($k_{\mathrm{B}}T/\varepsilon$ and $\rho\sigma^3$), and the calculation parameters–can be saved to a file on the user's computer and reloaded later within the applet. All numerical data can also be exported as tab-separated value (`.tsv`) text files.

3.2.1 System Information

Half of the interface is dedicated to receiving user input and displaying information about individual systems (see Fig. 3.1). This half of the interface features five sections: (a) controls for opening, closing, saving, or loading systems; (b) user input parameters; (c) a tabular pair potential; (d) buttons to trigger calculations; and (e) plots of the specified potential and its terraced

[1] Available online at <`http://docs.oracle.com/javase/tutorial/uiswing/index.html`>.
[2] Available online at <`http://www.jfree.org/jfreechart/`>.

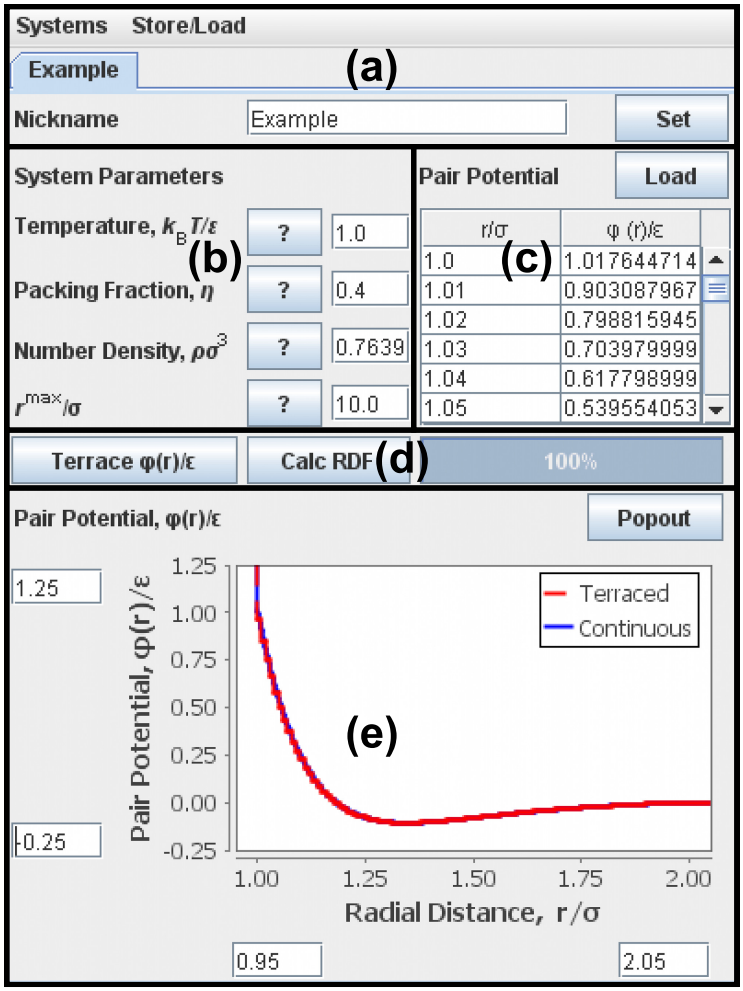

Figure 3.1: The system window in the applet for a selected example. (a) Systems can be loaded from and saved to local files; multiple system tabs can be present simultaneously and compared. Each system can be named descriptively. (b) Input parameters include the dimensionless temperature $k_\mathrm{B}T/\varepsilon$, the number density $\rho\sigma^3$ or packing fraction $\eta = \rho\pi\sigma^3/6$, and the outer range of the calculation, r^max/σ. (c) Each system's short-ranged contribution to the interaction potential can be input as a series of $[r/\sigma,\, \phi(r)]$ points, or loaded from a `.csv` file. (d) The terracing and RDF calculations are triggered with buttons, and calculation progress is displayed by the progress bar. (e) Both the continuous and terraced representations (see text) of the interaction potential are plotted for inspection.

representation.

Opening, closing, and naming systems. Each system has a nickname which appears throughout the applet. The applet begins with a single bare hard sphere system with the default nickname "System 1." The user can provide a new name in the `Nickname` field, then press `Set`. When multiple systems are open, the tabs at the top of the panel can be used to switch between the systems.

Through the `Systems` menu, the user can create additional empty systems or close the currently focused system tab. Through the `Store/Load` menu, the user can store the current system in a local file or import a previously saved system.

Input parameters. The user must specify the system's dimensionless temperature $k_{\mathrm{B}}T/\varepsilon$, either the number density $\rho\sigma^3$ or packing fraction $\eta = \rho\pi\sigma^3/6$, and the range of the calculation, $r^{\max}/\sigma$. Care should be taken to ensure that oscillations in the RDF have decayed before $r^{\max}/\sigma$. The theoretical approach from Chapter 2 that the applet relies upon, similar to most theories of simple liquids [31], loses accuracy near a critical point or in systems with very high density (e.g., $\rho\sigma^3 \gtrsim 1$) or very low temperature (e.g., $k_{\mathrm{B}}T/\varepsilon \lesssim 0.05$), with the details depending on the chosen interaction. For most state points away from the critical point of the fluid, the default choice of $r^{\max}/\sigma = 10$ is conservative. When either η or $\rho\sigma^3$ is changed, the other field updates automatically.

Interparticle pair potential. The short-ranged addition to the pair potential $\phi(r)$ can be provided either by editing a table within the applet or by loading the data from an external `.csv` file. For simple pair potentials constructed from line segments, like a ramp or Jagla potential [39], it is sufficient to specify only the end points of each segment. For more complex interactions, however, it is often more convenient to prepare the potential in a separate file using, e.g., a spreadsheet editing program, then press the `Load` button in the applet to import the pair potential data.

Performing calculations. Once inputs have been provided, the user may click either `Terrace φ(r)/ε` or `Calc RDF` to view the terraced pair potential or begin calculation of the radial distribution function, respectively. The user may proceed directly from providing inputs to calculating the RDF, but it is recommended that the terraced potential be generated and inspected before beginning the more intensive RDF calculations. The bar to the right of these buttons depicts the progress of the RDF calculation.

Plot of pair potentials. The continuous and terraced pair potentials are presented graphically for easy inspection. The continuous curve is updated in real-time as the pair potential is edited; the terraced representation is added when either of the calculation buttons is pressed. By default, the plot shows the full data sets; to focus on a region of interest, the user can click and drag a rectangle, or edit the values in the boxes along the axes to specify an

exact window. If desired, the chart can be reproduced in a separate window by pressing the `Popout` button. Many more charting options, built into the JFreeChart library, are available by right-clicking the plot.

3.2.2 Comparing Structure and Thermodynamics

The second half of the applet interface allows the user to view the calculated RDFs and compare them across multiple systems. This half contains sections for (a) selecting which systems and system data to compare; (b) plots of the selected RDF predictions; and (c) tabulated numerical data for the selected systems (see Fig. 3.2).

Selecting systems. Once a system's RDF calculation is complete, the user can choose to inspect the resulting $g_{\mathrm{ST}}(r)$ or $g(r)$ data by selecting the appropriate checkboxes. Multiple data series can be selected simultaneously so the user can compare different systems and analyze, e.g., the impact of the smoothing algorithm or the differences in RDF structure between two systems.

Plot of radial distribution functions. The selected radial distribution functions are presented graphically for immediate comparison. This plot functions identically to the pair potential plot described earlier.

Data tables. Numerical intermediate data are available in tabular form for all of the active systems, including continuous and terraced $\varphi(r)$ representations, and sawtoothed and smoothed RDFs. An additional table, labeled

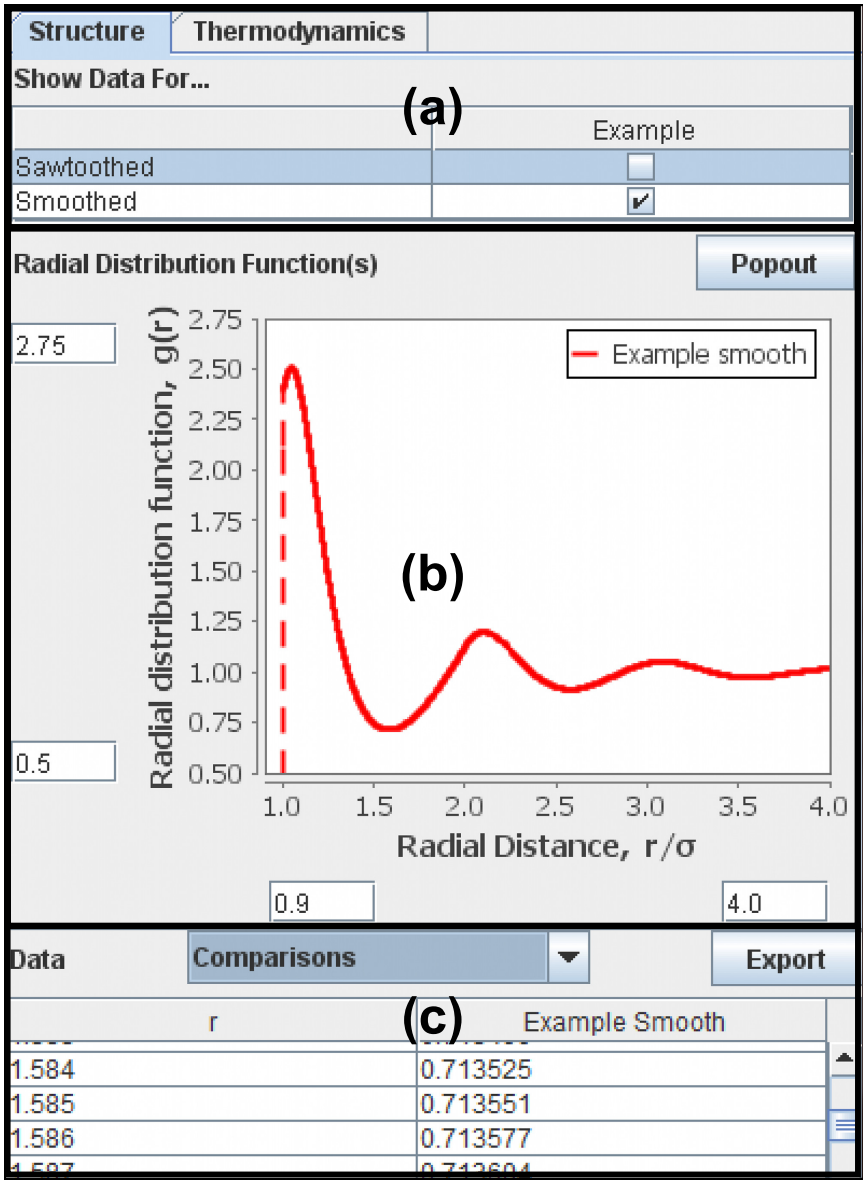

Figure 3.2: The sawtoothed and smoothed radial distribution functions for all systems currently calculated are available for comparison. (a) Each curve can be toggled on or off to facilitate comparisons between specific systems. The radial distribution functions are both (b) plotted graphically, for visual inspection, and (c) available as data series, to precisely compare specific values. The data series can also be exported as a `.tsv` file.

`Comparisons` in the drop-down box, contains all of the data series corresponding to the current state of the RDF plot. Any data in these data tables can be copied and pasted; or, the user can press the `Export` button to save the selected table as a tab-separated value (`.tsv`) file, which can then be manipulated with a text editing or spreadsheet program.

The `Thermodynamics` tab, not pictured, contains a table with the thermodynamic properties described in Section 3.1.2—average configurational energy, average internal energy, compressibility factor, and two-body excess entropy—calculated for each system. It also features togglable data series and can be used in the same ways as the RDF data tables described above.

3.3 Teaching Examples

This applet offers many pedagogical opportunities to teachers and students of classical statistical mechanics. Most simply, it can illustrate the effects of changing temperature, density, or interactions on the fly, e.g. during a lecture. The applet can also be used to prepare example figures through the use of the plot saving functionality available within the applet, or by exporting the calculated data and plotting in a preferred environment. Because of its ability to save and load states, an example "initial state" could be prepared for further manipulation during a lecture, or distributed as part of a homework assignment. Students are also able to experiment freely by modifying the attractions or repulsions, changing the density or temperature, etc., to develop an intuition for complex fluid phenomena, without needing a simulation suite

or more advanced statistical mechanics coding knowledge.

Here we provide examples of how our applet might be used to illustrate two fundamental ideas.

3.3.1 Emerging Coordination Shell Structure with Density

The hard sphere (HS) fluid—whose particles have no interaction other than a volume exclusion to prevent interparticle overlap, e.g. $\phi(r) = 0$ in Eq. (3.1)—is a canonical reference model for the structure of dense liquid and colloidal systems, and it is one of the simplest models of a non-ideal gas. Because the interaction potential is either infinite or zero, its structure is independent of temperature (as are its energies and dynamics, apart from a trivial scaling related to particle velocities) [31]. Despite their simplicity, hard sphere fluids (like atomic liquids and particle suspensions) develop nontrivial structure (e.g., interparticle correlations) as density increases. At $\eta \approx 0.494$, the HS fluid experiences a purely entropy-driven freezing transition to form an FCC crystal [31].

In Fig. 3.3, we have used the applet to plot the radial distribution functions of HS fluid systems at $\eta = 0.01$, 0.15, 0.30, and 0.45. As the packing fraction is increased, several trends can be readily observed: first, the range of the correlation increases from slightly beyond $r/\sigma = 1$ to nearly $r/\sigma = 5$ as coordination shells of nearest, next-nearest neighbors (and so on) develop; second, the magnitude of the first peak in the radial distribution function increases from $g(r) \approx 1$ to $g(r) \approx 5$, indicating that particles are contacting

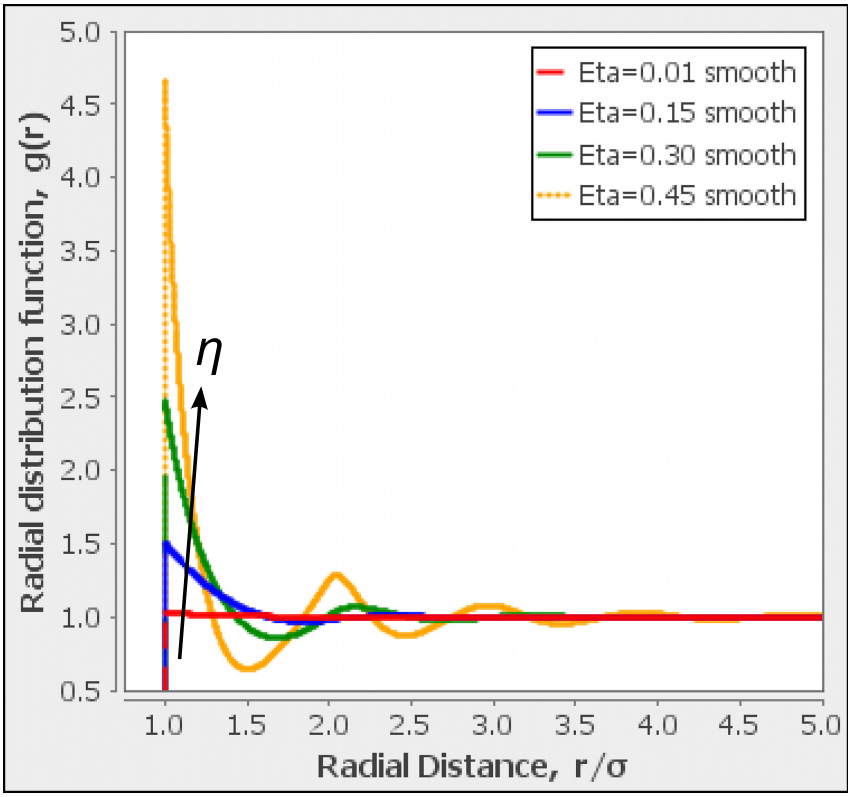

Figure 3.3: The amount of structure increases with increasing packing fraction in a hard sphere fluid; shown are packing fractions $\eta = 0.01$ (red), where almost no correlations are present beyond the hard core; $\eta = 0.15$ (blue); $\eta = 0.30$ (green); and $\eta = 0.45$ (orange), where correlations extend to nearly six particle diameters and a large population of particles are in contact.

one another with greater and greater frequency; and third, the period of the oscillations (once they are present) shrinks as the coordination shells become more condensed. These structural trends with increasing density, also commonly seen in simple liquids, result in an increased pressure and reduced excess entropy–both of which are readily verifiable in the applet.

3.3.2 Temperature Effects in a Two-Length-Scale Fluid

In liquids more complex than hard spheres, multiple length scales can be present within the pair potential. For example, in a repulsive ramp system where

$$\phi(r) = 2 - \frac{r}{\sigma}, \tag{3.7}$$

there are relevant length scales at $r/\sigma = 1$, at the edge of the hard core, and at $r/\sigma = 2$, at the outer limit of the interaction (see Fig. 3.4). For an interaction of this form, one might expect that at high temperatures ($k_{\mathrm{B}}T \gg \varepsilon$), the energy associated with the finite repulsion outside $r = \sigma$ would be negligible relative to the thermal energy of the system; therefore, the hard core length scale might be most relevant (i.e, the system approaches hard-sphere-like structure). Conversely, at low temperatures ($k_{\mathrm{B}}T \ll \varepsilon$), contributions from the finite repulsion would be more significant, leading the $r = 2\sigma$ (more open, low density) length scale to dominate.

The applet can be used to demonstrate this phenomenon, by simulating the same ramp potential at a series of different temperatures, $k_{\mathrm{B}}T/\varepsilon = 0.2$, 0.4, 0.6, 0.8, and 1.0 (see Fig. 3.5). At all of these temperatures, clear strong

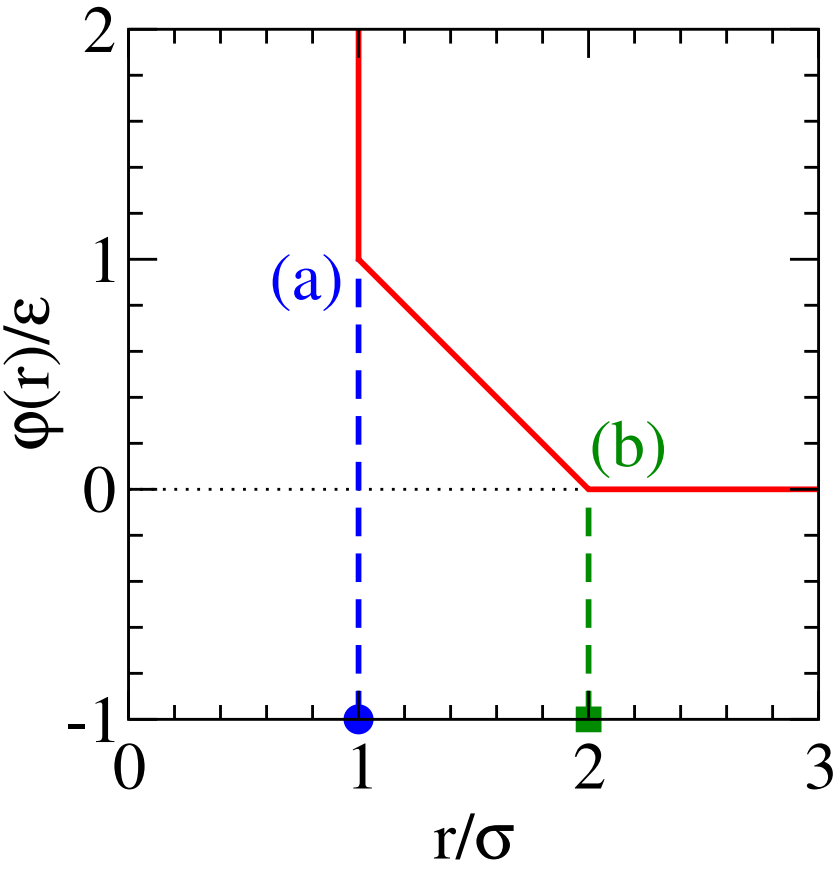

Figure 3.4: The repulsive ramp potential (red solid curve) has two length scales: the hard core diameter (a, blue circle), and the outer edge of the ramp (b, green square). The former is favored at high temperature, while the latter is favored at low temperature.

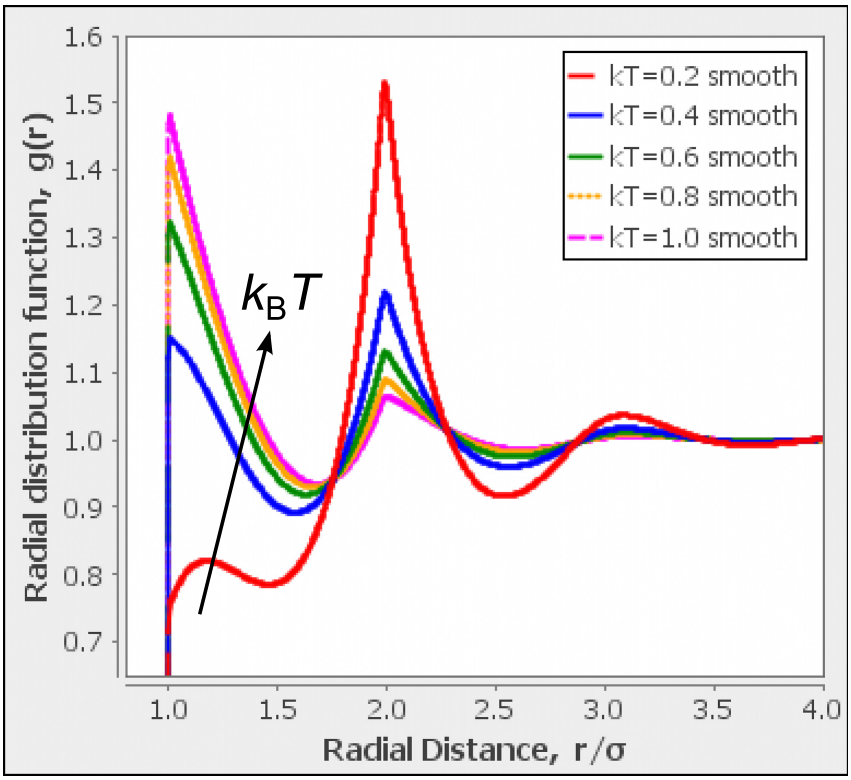

Figure 3.5: Smoothed radial distribution functions of ramp systems (see Eq. (3.7)) plotted with the applet, where $\eta = 0.2$ and $k_B T = 0.2$ (red), 0.4 (blue), 0.6 (green), 0.8 (orange), and 1.0 (magenta).

peaks corresponding to the two length scales in the pair potential are present at $r/\sigma = 1$ and $r/\sigma = 2$. However, as the temperature decreases, so too does the significance of the inner peak; below $k_{\mathrm{B}}T/\varepsilon = 0.6$, the outer peak is taller.

These temperature-dependent trends are analogous to those seen in network-forming fluids like liquid water, where the hydrogen-bond network energetically favors low-coordinated, open structures. Due to analogous physics along isobars, at moderate pressures, such structures dominate in water, leading the fluid to exhibit negative thermal expansivity (expansion upon cooling) at low temperature–a thermodynamic property also exhibited by the ramp model [24, 39, 71]. Similar features occur in other network forming fluids like silica whose interactions energetically favor locally open structures as well.

3.4 Conclusion

This applet provides new opportunities for students and teachers of statistical mechanics to explore and develop a deeper conceptual understanding of the effects of interparticle interactions and the thermodynamic state on the particle-scale equilibrium structure and thermodynamic properties in a fluid system.

The applet is freely available for use or download at <`http://www.truskettgroup.com/fluidapp/`>, and its source code is available under the GNU General Public License[3] on GitHub.[4] The authors encourage any in-

[3]License text available online at <`http://www.gnu.org/copyleft/gpl.html`>.
[4]Available online at <`https://github.com/TRP3/FluidRDFApp`>.

terested parties to modify or expand the applet in useful ways. We hope to expand its functionality in the future, most immediately by adding options for the use of additional integral equation theory closures in order to treat an even broader variety of possible pair interactions. We also intend to implement a calculation of the structure factor,

$$S(k) = 1 + 4\pi\rho \int_0^\infty \frac{\sin(kr)}{kr} \left[g(r) - 1\right] r^2 \, dr, \tag{3.8}$$

which is an experimentally accessible quantity that can offer insight into, e.g., freezing transitions via the Hansen-Verlet freezing criterion [32].

Chapter 4

Predicting the structure of fluids with piecewise constant interactions: Comparing the accuracy of five efficient integral equation theories

For bulk fluids, a key aim for property prediction is to discover the one-to-one link [35] between $g(r)$, the radial distribution function (RDF) of a system at a given set of conditions, and $\varphi(r)$, the interparticle pair potential. Knowledge of these functions of interparticle separation r allows for the direct calculation of the static structure factor, the energy, the pressure, and the isothermal compressibility [31]. Estimations of other properties can be directly obtained from knowledge of the RDF as well. One example is the two-body excess entropy, which is often a good approximation of the total excess entropy [50] for simple liquids. Another is the information-theoretic estimate for the probability $p_n(\Omega)$ of observing n particle centers in a molecular-scale subvolume Ω, a quantity which characterizes the fluid's density fluctuations [38]. Excess entropy, its two-body approximation, and p_0 have been shown to correlate with various dynamic properties of equilibrium fluids, e.g. diffusivity or viscosity [1–4, 12, 15, 18, 22, 28, 30, 42, 43, 48, 51, 52, 56, 57, 60]. Mode-coupling theory also predicts that dynamic phenomena can be directly esti-

mated from knowledge of the static structure factor [54].

With these considerations in mind, in this chapter we use molecular simulations to test the accuracy of RDF predictions for five approximate integral-equation theory closures: Percus-Yevick, hypernetted chain and reference hypernetted chain [31], first-order mean spherical approximation (FMSA) [65], and a modified exponential version of FMSA [36]. Other more resource-intensive theories, like the Rogers-Young and hybrid mean-spherical approximations [55, 75], self-consistent Ornstein-Zernike approaches [31], and thermodynamic perturbation theories [61, 76, 77] are not considered here. We apply the simpler five theories listed above to a diverse suite of eight pair potentials previously introduced by Santos et al [59], each composed of a hard core at $r = \sigma$ plus two piece-wise constant sections at larger r (i.e. wells or shoulders), that qualitatively mimic some of the features observed in the effective interactions of complex fluid systems. For each interaction, we investigate four thermodynamic state points with various combinations of low and high density and low and high temperature, and we compare the theoretical predictions for the RDF, the energy, and the two-body excess entropy to data from event-driven molecular dynamics simulations. To facilitate the RDF comparisons we introduce a "cumulative squared error" metric, which provides a quantitative characterization of the overall quality of each theoretical prediction. We also assess the accuracy of predictions for the potential energy and the two-body excess entropy.

4.1 Methods

4.1.1 Integral Equation Theory

Integral equation theories for uniform, isotropic fluids typically involve solving a system of two equations: the Ornstein-Zernike relation,

$$h(r) = c(r) + \rho \int c\left(|\mathbf{r}' - \mathbf{r}|\right) h(r') d\mathbf{r}', \tag{4.1}$$

which defines the direct correlation function $c(r)$ in terms of the number density ρ and the total correlation function $h(r) = g(r) - 1$, and a closure, e.g.,

$$h(r) + 1 = \exp\left[-\beta\varphi(r) + h(r) - c(r) + B(r)\right], \tag{4.2}$$

which introduces the link to the pair potential $\varphi(r)$, where $\beta = (k_{\mathrm{B}}T)^{-1}$, T is temperature, k_{B} is Boltzmann's constant, and $B(r)$ is the so-called bridge function.

Two common approximations for $B(r)$ are the Percus-Yevick (PY) closure,

$$B_{\mathrm{PY}}(r) = \ln\left[h(r) - c(r) + 1\right] - h(r) + c(r), \tag{4.3}$$

and the hypernetted chain (HNC) closure,

$$B_{\mathrm{HNC}}(r) = 0. \tag{4.4}$$

Another is the so-called reference hypernetted chain approximation (RHNC), which assumes that the bridge function can be accurately approximated by that of a reference fluid, typically one of hard spheres at the same density:

$$B_{\mathrm{RHNC}}(r) = B_{\mathrm{HS}}(r). \tag{4.5}$$

The hard-sphere fluid's bridge function $B_{\mathrm{HS}}(r)$ has been calculated through careful molecular simulations, and multiple parameterizations for its density dependence exist [34, 47, 68]. For this work, we employ the analytical parameterization proposed by Malijevský and Labík [47] for the RHNC closure.

With $B(r)$ specified by these closures, we solve the coupled equations (4.1) and (4.2) using a rapidly-converging combination of Newton-Raphson and Picard root-finding methods developed by Labík et al. [44].

An alternative strategy is to replace the closure of Eq. 4.2 with separate expressions. For example, the mean spherical approximation (MSA) assumes the following relations hold,

$$\begin{aligned} g_{\mathrm{MSA}}(r) &= 0 \qquad r < \sigma, \\ c_{\mathrm{MSA}}(r) &= 0 \qquad r \geq \sigma. \end{aligned} \tag{4.6}$$

By further assuming first-order expansions in the characteristic dimensionless energy of the potential $\beta\varepsilon$ for both $g(r)$ and $c(r)$–e.g., $g_{\mathrm{FMSA}}(r) = g_{\mathrm{HS}}(r) + \beta\varepsilon g_1(r)$, where $g_{\mathrm{HS}}(r)$ is the pair correlation function for a hard sphere system at the same density–Tang and Lu closed the equations analytically for several common pair interactions, including square wells [65]. We refer to this solution as the first-order mean spherical approximation (FMSA). In principle, FMSA can be applied to potentials with square shoulders as well. But for strong interactions, FMSA is known to incorrectly predict RDFs with negative values for some interparticle separations [36]. To resolve this, Hlushak et al. modified the FMSA to make it equally applicable to wells and shoulders by rearranging the terms in the series expansion, so that $g_{\mathrm{EFMSA}}(r) = g_{\mathrm{HS}}(r)\exp[-\beta\varepsilon g_1(r)]$ [36].

In this work, we refer to this analytical solution as the exponential first-order mean spherical approximation (EFMSA).

4.1.2 Suite of Two-Step Potentials

Motivated by Santos et al. [59], we examine predictions for fluids from a set of pair interactions comprising a hard core and two piecewise-constant steps,

$$\varphi(r) = \begin{cases} \infty & r < \sigma, \\ \varepsilon_1 & \sigma \leq r < \lambda_1, \\ \varepsilon_2 & \lambda_1 \leq r < \lambda_2, \\ 0 & r \geq \lambda_2, \end{cases} \tag{4.7}$$

where ε_1 and ε_2 are the energies of the first and second steps, respectively, and λ_1 and λ_2 are the outer edges of the first and second steps, respectively.

Furthermore, as in Santos et al., we restrict the values of ε_i to the set $\{-\varepsilon, -\varepsilon/2, 0, \varepsilon/2, \varepsilon\}$, where ε is a characteristic energy scale. Cases where $\varepsilon_1 = \varepsilon_2$ or $\varepsilon_2 = 0$ reduce to either single square wells or shoulders, or hard spheres, which have all been studied extensively elsewhere (see, e.g., refs. 1-41 in [74]) and are not considered here. We also exclude cases where $\max\{|\varepsilon_1|, |\varepsilon_2|\} = \varepsilon/2$. Of the cases where ε_1 and ε_2 have opposite sign, we consider only combinations where $\varepsilon_2 = -\varepsilon_1 = \pm\varepsilon$. We choose $\lambda_1 = 1.5\sigma$ and $\lambda_2 = 2\sigma$ in order to provide challenging perturbations to the bare hard sphere system that are still amenable to molecular simulation and theoretical treatment. After imposing these restrictions, the remaining eight pairwise interactions shown in Fig. 4.1, which we refer to as "Type A–H," form our test suite.

To explore how the accuracy of the various theories varies with den-

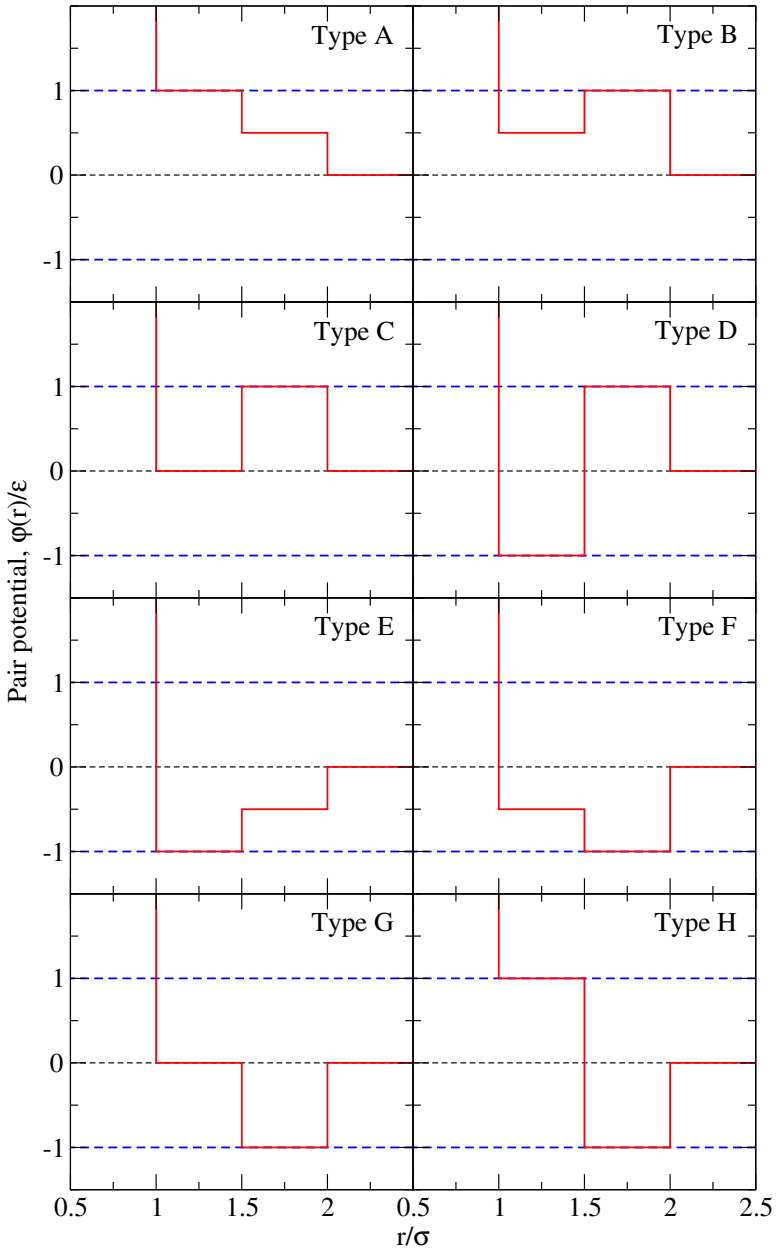

Figure 4.1: The suite of eight pair interactions considered in this study, inspired by Santos et al. [59], is topologically exhaustive (e.g., there are no other qualitative arrangements of two constant pairwise pieces that are not more appropriately labeled single wells or shoulders).

sity and temperature, we investigate each interaction at the four state points comprising combinations of packing fraction $\eta = \rho\pi\sigma^3/6 = 0.15$ or 0.45 and dimensionless temperature $T^* = k_\mathrm{B}T/\varepsilon = 0.67$ or 2.0.

4.1.3 Molecular Simulations

We compare the theoretical predictions for the RDF, the energy, and the two-body excess entropy to the results of event-driven molecular dynamics simulations performed with the DynamO simulation engine [10]. Periodic boundary conditions were used, and the simulated systems were sized such that adequate RDF statistics could be collected for separations up to at least $r = 10\sigma$. In practice, this required $N = 4000$ particles when $\eta = 0.15$, and $N = 8788$ particles when $\eta = 0.45$. The "bins" for particle counts were 0.005σ wide. Temperatures were set and maintained using an Andersen thermostat [6].

Each simulation was initialized as an FCC lattice of the desired density at a high temperature, with randomly assigned particle velocities. After equilibrating for ten million events, the simulations were cooled to the desired temperature and re-equilibrated for a further ten million events. Then, the thermostat was removed, and the RDF was measured over the final five million events.

4.1.4 Quantifying Error in Predictions

To compare the various RDF theoretical predictions to simulations at a given state point, we define a metric we call the cumulative squared error, CSE(r):

$$\mathrm{CSE}(r) = \frac{\int_\sigma^r \left[h_{\mathrm{sim}}(r') - h_{\mathrm{thy}}(r')\right]^2 r'^2\, dr'}{\int_\sigma^\infty h_{\mathrm{sim}}^2(r') r'^2\, dr'}. \tag{4.8}$$

The integrand in the numerator characterizes the squared deviation in the total correlation function between the prediction of a given theory $h_{\mathrm{thy}}(r)$ and the result of the 'exact' simulation $h_{\mathrm{sim}}(r)$; the power of two eliminates any possible cancellation of error, e.g. for cases where a theory both underpredicts and overpredicts the value of $h(r)$ at different values of r. The denominator accumulates the total squared correlations in the simulated system, and thus normalizes the overall function to facilitate comparison between systems with different degrees of correlation (e.g., between low-density and high-density systems).

As r approaches infinity, all $h(r)$ curves converge to zero and the CSE converges to a finite value, CSE_∞:

$$\mathrm{CSE}_\infty = \lim_{r\to\infty} \mathrm{CSE}(r), \tag{4.9}$$

which is a measure of the summed squared correlations as a fraction of the total squared correlations in the system; thus, a larger value of CSE_∞ indicates that a theoretical prediction deviates more significantly from the "exact" simulation

results. By construction, CSE_∞ has a defined minimum of 0 and, while it does not have a rigorous maximum, its value is typically less than 1 except in cases where the theoretical predictions are qualitatively very poor.

We also calculate the potential energy per particle U/ε,

$$\frac{U}{\varepsilon} = \frac{\rho}{2} \int_0^\infty \frac{\varphi(r)}{\varepsilon} g(r)\, d\mathbf{r}, \tag{4.10}$$

and the two-body contribution to excess entropy $s^{(2)}/k_\mathrm{B}$,

$$\frac{s^{(2)}}{k_\mathrm{B}} = -\frac{\rho}{2} \int_0^\infty \left[g(r) \ln g(r) - g(r) + 1 \right]\, d\mathbf{r}, \tag{4.11}$$

from simulations and theoretical predictions. Both quantities can also be directly computed from $g(r)$ and thus, the normalized absolute deviation of the predicted versus simulated values can be used as an indication of the success of theoretical predictions. However, note that different RDFs can, in principle, give rise to the same value of U/ε or $s^{(2)}/k_\mathrm{B}$. Moreover, U/ε only depends on correlations within the range of the pair interaction. As a result, we argue here that since the RDF is weighted differently for each thermodynamic quantity, the CSE metric we introduce–which tests the overall similarity between predicted and simulated RDFs–represents a more sensitive measure for the overall predictive quality of a particular theory.

4.2 Results and Discussion

Structural predictions for the Type A pair interaction are compared to simulation results in Fig. 4.2, along with the corresponding cumulative

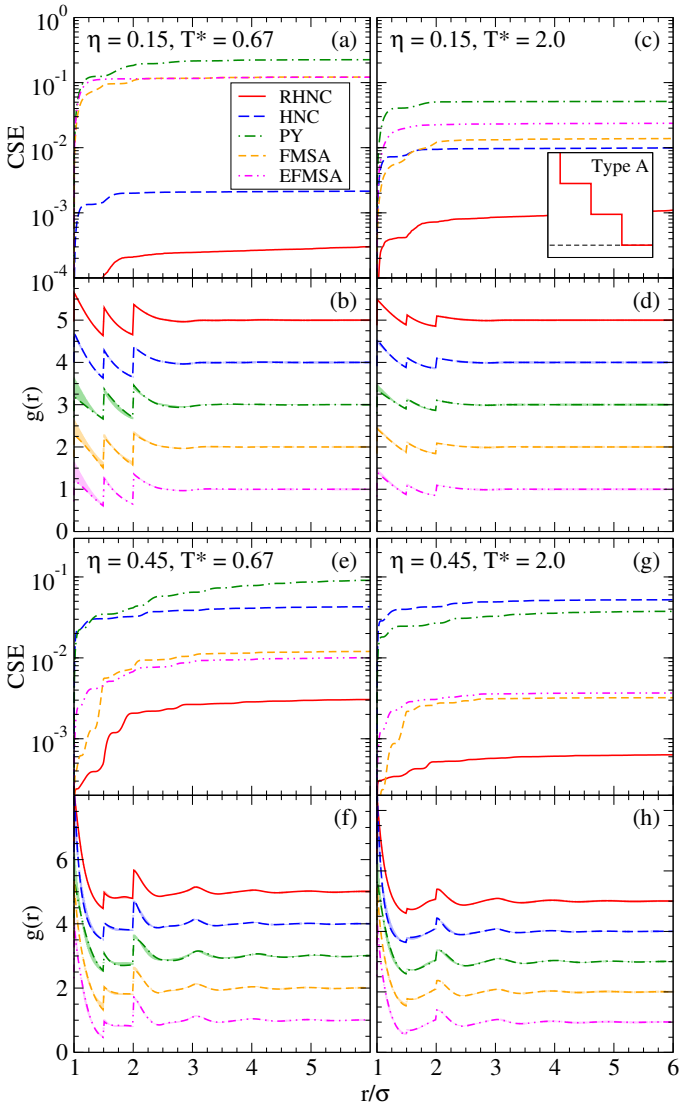

Figure 4.2: Radial distribution functions $g(r) = h(r) + 1$ and the associated cumulative squared errors (CSE, see Eq. (4.8)) predicted by the reference hypernetted chain (RHNC), hypernetted chain (HNC), and Percus-Yevick (PY) Ornstein-Zernike closures [31, 47]; the first-order mean spherical approximation solution (FMSA) [65]; and the simple exponential first-order mean spherical approximation (EFMSA) [36], for the "type A" pair interaction. Shaded regions adjacent to each $g(r)$ indicate the difference between the theory and simulation results.

squared errors as calculated via Eq. (4.8). For this interaction, the analytic solutions (FMSA and EFMSA) perform better at higher rather than at lower equilibrium fluid densities. As density increases, the effect of the excluded volume captured by the well-modeled hard-sphere RDF, $g_{\mathrm{HS}}(r)$, overwhelm the energetic perturbations from the repulsive steps and dominate the resulting structure. Of the tested integral-equation theories with simple numerical closures, the PY closure tends to perform least well near contact, and for interaction Type A, the RHNC offers the best predictions at all four state points investigated. Analogous figures for each of the other interactions are presented for the interested reader in Appendix B.

It is tempting to conclude from a visual comparison of theoretical and simulated radial distribution functions that all of the theories perform similarly well, especially at the higher temperature (Figs. 4.2d and 4.2h). However, the resulting CSEs differ *by nearly two orders of magnitude* from most to least accurate (Figs. 4.2c and 4.2g), which underscores the utility and sensitivity of the CSE metric. As discussed below, these differences in the CSE become important when computing other quantities that depend on the RDF, especially when one considers that each thermodynamic quantity weights the RDF in a different way.

The total cumulative squared errors CSE_∞ for all interactions, state points, and theories are listed in Table 4.1. Six of the total thirty-two combinations of interaction type and state point considered did not produce single-phase, uniform fluids when simulated. Of the remaining twenty-six systems,

Table 4.1: Total cumulative squared errors (CSE_∞) for all theoretical approaches, thermodynamic state points, and interactions considered. "R," "H," and "P" are the RHNC [31, 47], HNC [31], and PY [31] closures to the Ornstein-Zernike relation, respectively. "F" is the FMSA [65], and "E" is the EFMSA [36]. Italics indicate the lowest value of CSE_∞ (and hence the theory with the most accurate structural prediction) at each combination of state point and interaction type.

	Type A				Type B			
T^*	0.67		2.00		0.67		2.00	
η	0.15	0.45	0.15	0.45	0.15	0.45	0.15	0.45
R	*0.000*	*0.003*	*0.002*	*0.001*	*0.001*	*0.011*	*0.000*	*0.002*
H	0.002	0.043	0.010	0.052	0.001	0.037	0.001	0.057
P	0.225	0.095	0.052	0.038	0.013	0.021	0.005	0.007
F	0.122	0.012	0.014	0.003	0.092	0.053	0.010	0.006
E	0.121	0.010	0.024	0.004	0.082	0.098	0.008	0.011

	Type C				Type D			
T^*	0.67		2.00		0.67		2.00	
η	0.15	0.45	0.15	0.45	0.15	0.45	0.15	0.45
R	*0.002*	*0.010*	*0.000*	*0.003*	*0.079*	0.047	*0.001*	*0.004*
H	0.003	0.022	0.001	0.059	0.082	*0.031*	0.002	0.055
P	0.005	0.019	0.001	0.003	0.092	0.203	0.002	0.020
F	0.096	0.082	0.008	0.009	0.168	0.276	0.016	0.018
E	0.184	0.159	0.015	0.016	0.411	0.524	0.040	0.032

	Type E				Type F			
T^*	0.67		2.00		0.67		2.00	
η	0.15	0.45	0.15	0.45	0.15	0.45	0.15	0.45
R	–[a]	–[a]	–[a]	*0.001*	–[a]	0.082	–[a]	*0.004*
H	–[a]	–[a]	–[a]	0.067	–[a]	*0.027*	–[a]	0.049
P	–[a]	–[a]	–[a]	0.020	–[a]	0.255	–[a]	0.045
F	–[a]	–[a]	–[a]	0.004	–[a]	0.275	–[a]	0.026
E	–[a]	–[a]	–[a]	0.002	–[a]	0.113	–[a]	0.012

	Type G				Type H			
T^*	0.67		2.00		0.67		2.00	
η	0.15	0.45	0.15	0.45	0.15	0.45	0.15	0.45
R	–[a]	0.018	*0.001*	*0.006*	*0.052*	0.043	*0.004*	*0.012*
H	–[a]	*0.011*	0.008	0.041	0.063	*0.026*	0.008	0.029
P	–[a]	0.391	0.007	0.087	0.104	0.820	0.008	0.204
F	–[a]	0.253	0.018	0.038	0.208	0.526	0.032	0.078
E	–[a]	0.196	0.020	0.020	0.750	0.485	0.044	0.048

[a]Simulated system is not a single-phase, uniform fluid at equilibrium.

the RHNC offered the most accurate structural predictions for all but four; however, at three of these four points, the CSE_∞ of the RHNC is still within ca. 65% of the most accurate theory (HNC). All four points are at low temperature ($T^* = 0.67$) and high packing fraction ($\eta = 0.45$), and each of the pair interactions include attractions (types D, F, G, and H).

We also compare CSE_∞ against the absolute normalized errors for predictions of two example thermodynamic quantities, two-body excess entropy $s^{(2)}/k_\mathrm{B}$ and potential energy U/ε, in Fig. 4.3. Fig. 4.3a shows that CSE_∞ is generally a good predictor of $s^{(2)}/k_\mathrm{B}$ accuracy, although there are a handful of instances where the fractional error in the excess entropy is low while CSE_∞ is higher.The correlation between CSE_∞ and the potential energy is weaker, but still present; this is likely due to opportunities for fortuitous cancellation of error when pair interactions contain both positive and negative contributions (e.g., types D and H), when portions of the interactions are zero (types C and G), or when significant contributions to CSE_∞ occur beyond the range of the pair interaction. Overall, however, it is clear that the accuracies of both example thermodynamic quantity predictions correlate well with the cumulative squared error. For the interested reader, the values of $\left|\left(s^{(2)}_\mathrm{thy}/s^{(2)}_\mathrm{sim}\right) - 1\right|$ and $|(U_\mathrm{thy}/U_\mathrm{sim}) - 1|$ are tabulated in Appendix C. If other thermodynamic quantities that depend on the RDF in a different way (e.g., the pressure or the isothermal compressibility) are also of interest, then the necessity to have an independent structural metric like CSE_∞ to assess the quality of the structural predictions is even more critical.

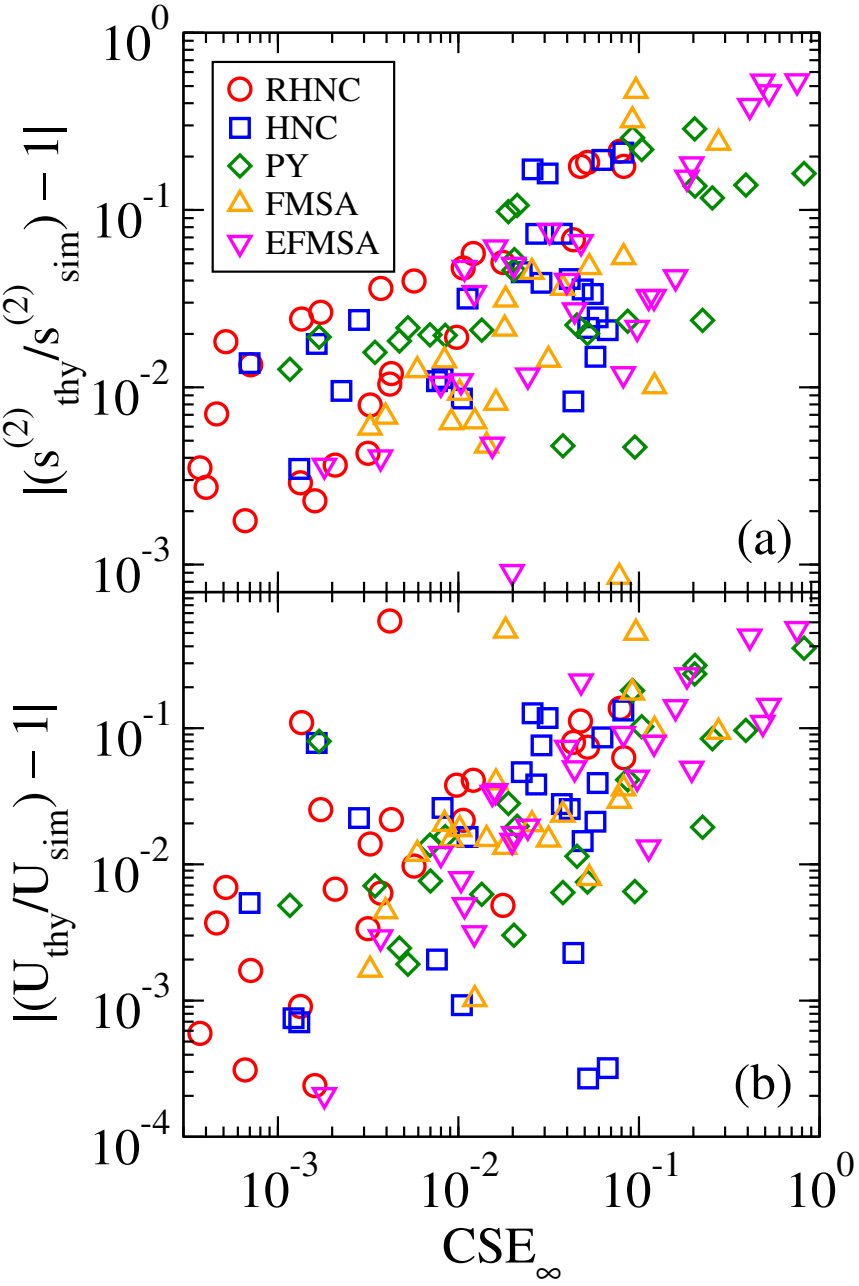

Figure 4.3: Correlations between total cumulative squared error CSE_∞ and either (a) absolute normalized two-body excess entropy error or (b) absolute normalized potential energy error for all data collected.

4.3 Conclusion

In order to quantify the overall accuracy of theoretical predictions for fluid structure, we have introduced the total cumulative squared error (CSE_∞) metric, which accumulates squared discrepancies between a theoretical prediction and a reference "exact" result at all separation distances along the total correlation function and avoids any possible cancellation of error. We find that this CSE_∞ metric is very sensitive and tends to forecast the overall accuracy of structure-dependent thermodynamic calculations. As a result, it is an excellent tool for comparing accuracy between multiple theories, particularly when differences are difficult to discern by visual inspection.

We have used this metric to test the performance of five integral equation theory-based approaches for predicting equilibrium fluid structure in systems with pair interactions comprising a hard core plus two piecewise constant interactions, and we find that the reference hypernetted chain (RHNC) integral equation closure offers accurate and efficient predictions across a broad range of interactions and thermodynamic state points. This kind of analysis, i.e., considering the accuracy of various efficient theoretical methods for predicting the structure consistent with a broad range of possible interactions, will be particularly important for inverse design problems where the goal is to rather accurately predict which interaction is consistent with a targeted structure (or structurally-related property).

Appendices

Appendix A

Choosing the maximum energy step size for a discretized potential

Choosing the maximum energy step size $\beta\Delta\epsilon^{max}$ requires some care. Radial distribution functions and internal energies at the weakest and strongest interactions for each model are presented below in Figures A.1 and A.2, respectively, for $\beta\Delta\epsilon^{max} = 0.05$, 0.1, 0.2, and 0.5. It can be seen that this strategy's predictions converge as $\beta\Delta\epsilon^{max}$ is made smaller. The invariance to further refinement for $\beta\Delta\epsilon^{max} \leq 0.2$ illustrates that our choice of $\beta\Delta\epsilon^{max} = 0.05$ in the main text is a conservative one.

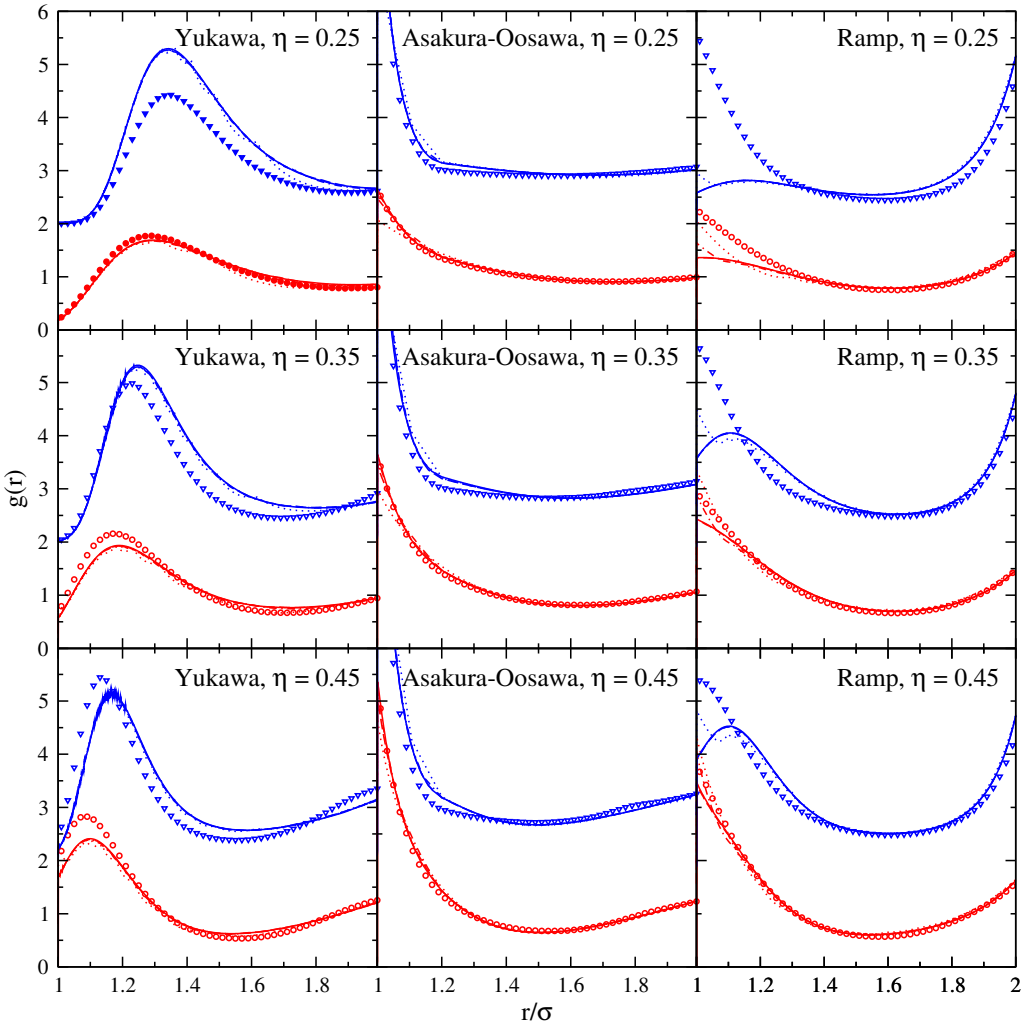

Figure A.1: Radial distribution functions of fluids with particles interacting via hard-sphere plus Yukawa repulsions, Asakura-Oosawa (AO) depletion attractions, and ramp-shaped repulsions at packing fractions $\eta = 0.25$, 0.35, and 0.45. Shown are predictions of Eq. (4) for $\beta\Delta\epsilon^{max} = 0.5$ (dotted lines), 0.2 (dash-dotted lines), 0.1 (dashed lines), and 0.05 (solid lines) and results of Monte Carlo simulations (symbols). For the Yukawa repulsions, $\kappa = 5$ and $\beta\gamma = 5$ (red) or 15 (blue). For the AO depletion attraction, $q = 0.2$ and $\eta_p = 0.04$ (red) or 0.2 (blue). For the repulsive ramp interaction, $r_c = 2\sigma$ and $\beta U_1 = 10$ (red) or 30 (blue). Curves for different interaction strengths are shifted vertically by integer values for clarity.

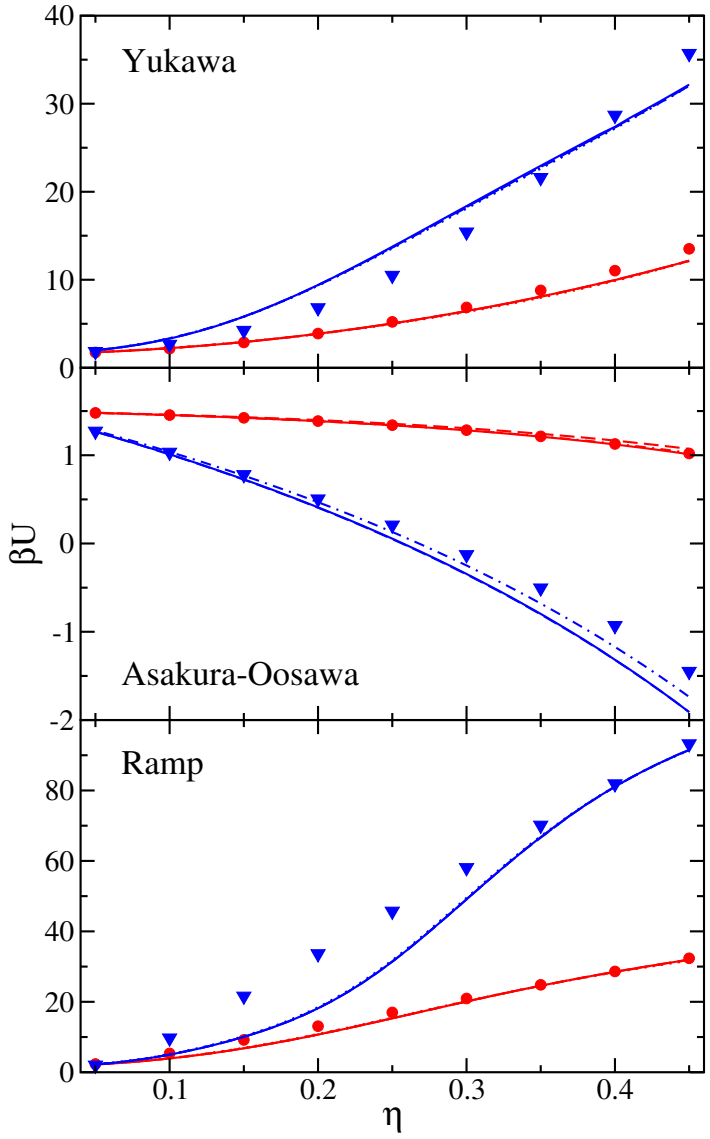

Figure A.2: Potential energy βU versus packing fraction η for fluids with particles interacting via hard-sphere plus Yukawa repulsions, Asakura-Oosawa (AO) depletion attractions, and ramp-shaped repulsions. Solid curves are obtained from the predicted RDFs for $\beta\Delta\epsilon^{max} = 0.5$ (dotted lines), 0.2 (dash-dotted lines), 0.1 (dashed lines), and 0.05 (solid lines), and symbols are results from Monte Carlo simulations. Interaction potential parameters for each system ($\beta\gamma$, ϕ_p, and βU_1) are the same as in Fig. 2.2.

Appendix B

Extended Type B-H Structure Plots

The predicted radial distribution functions $g(r)$ compared against simulation results, and the resulting cumulative squared errors CSE(r), are shown for interaction types B through H in Figs. B.1–B.7, respectively.

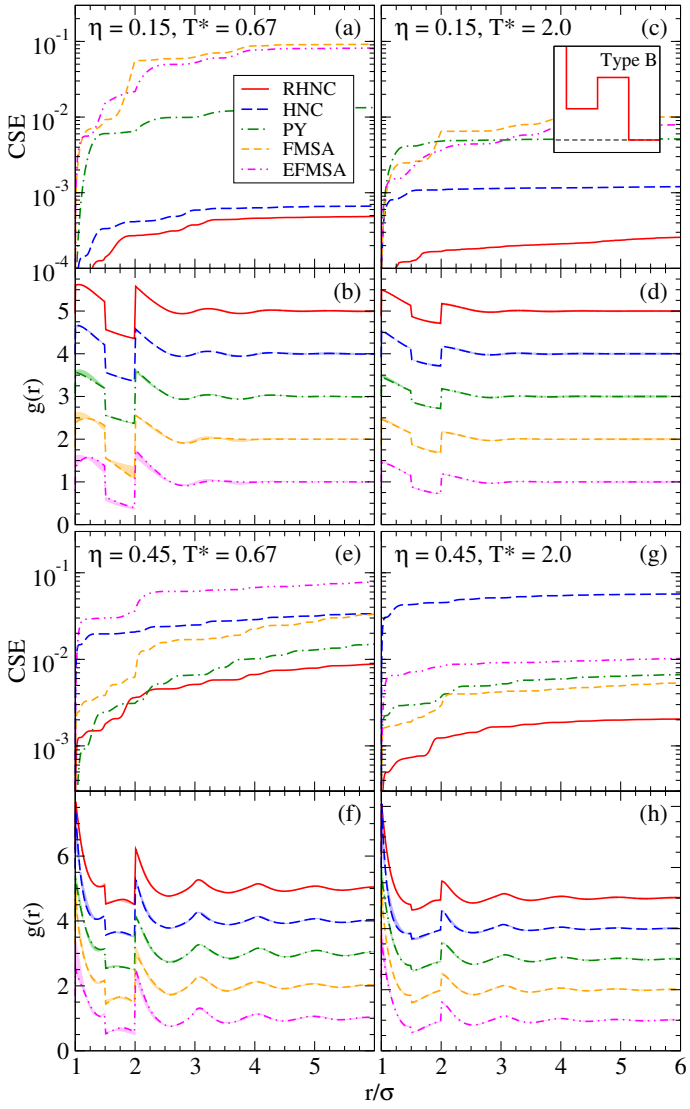

Figure B.1: Radial distribution functions $g(r) = h(r) + 1$ and the associated cumulative squared errors (CSE, see Eq. (4.8)) predicted by the reference hypernetted chain (RHNC), hypernetted chain (HNC), and Percus-Yevick (PY) Ornstein-Zernike closures [31, 47]; the first-order mean spherical approximation solution (FMSA) [65]; and the simple exponential first-order mean spherical approximation (EFMSA) [36], for the "Type B" pair interaction. Shaded regions adjacent to each $g(r)$ indicate the difference between the theory and EDMD simulation results.

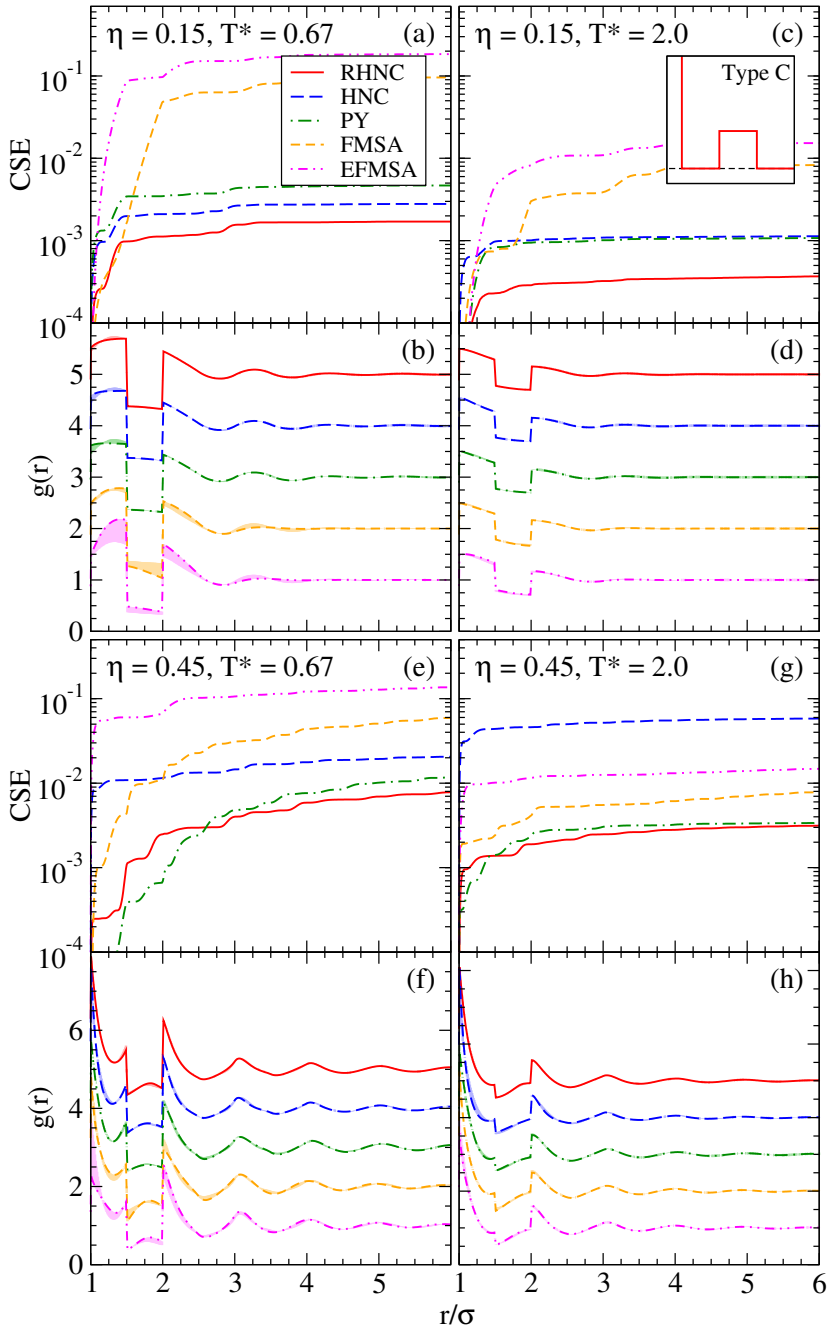

Figure B.2: Radial distribution functions and cumulative squared errors for the "Type C" pair interaction. Series are as in Fig. B.1.

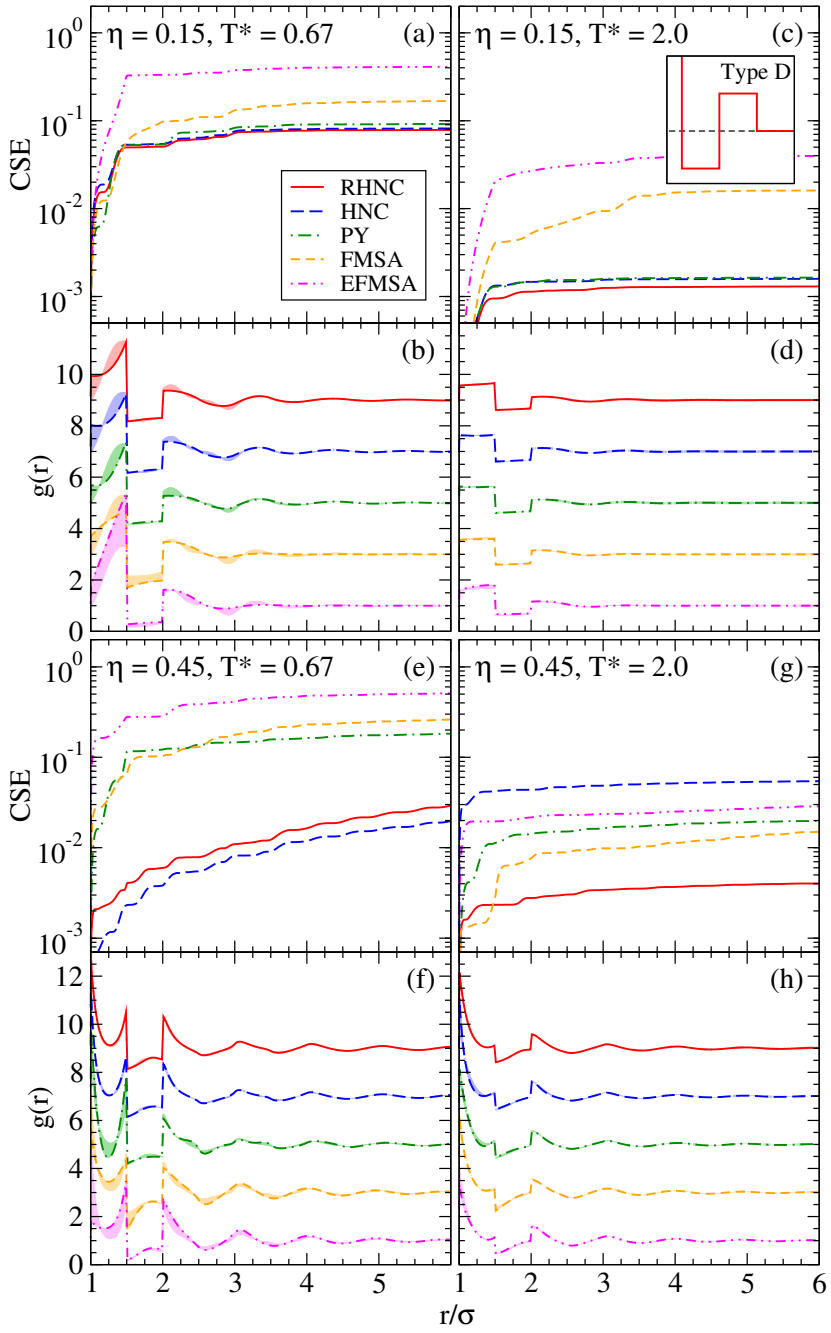

Figure B.3: Radial distribution functions and cumulative squared errors for the "Type D" pair interaction. Series are as in Fig. B.1.

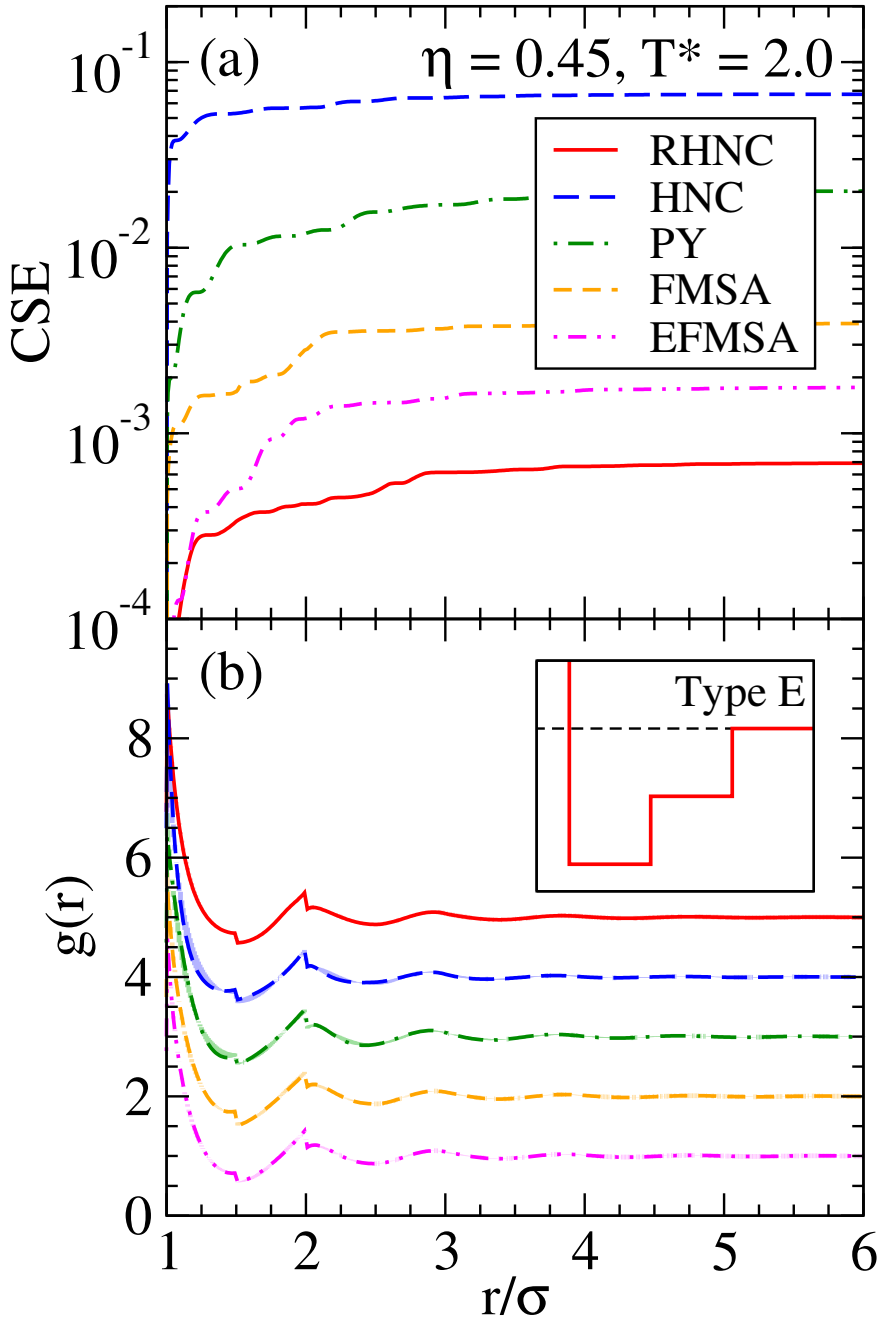

Figure B.4: Radial distribution functions and cumulative squared errors for the "Type E" pair interaction. Series are as in Fig. B.1.

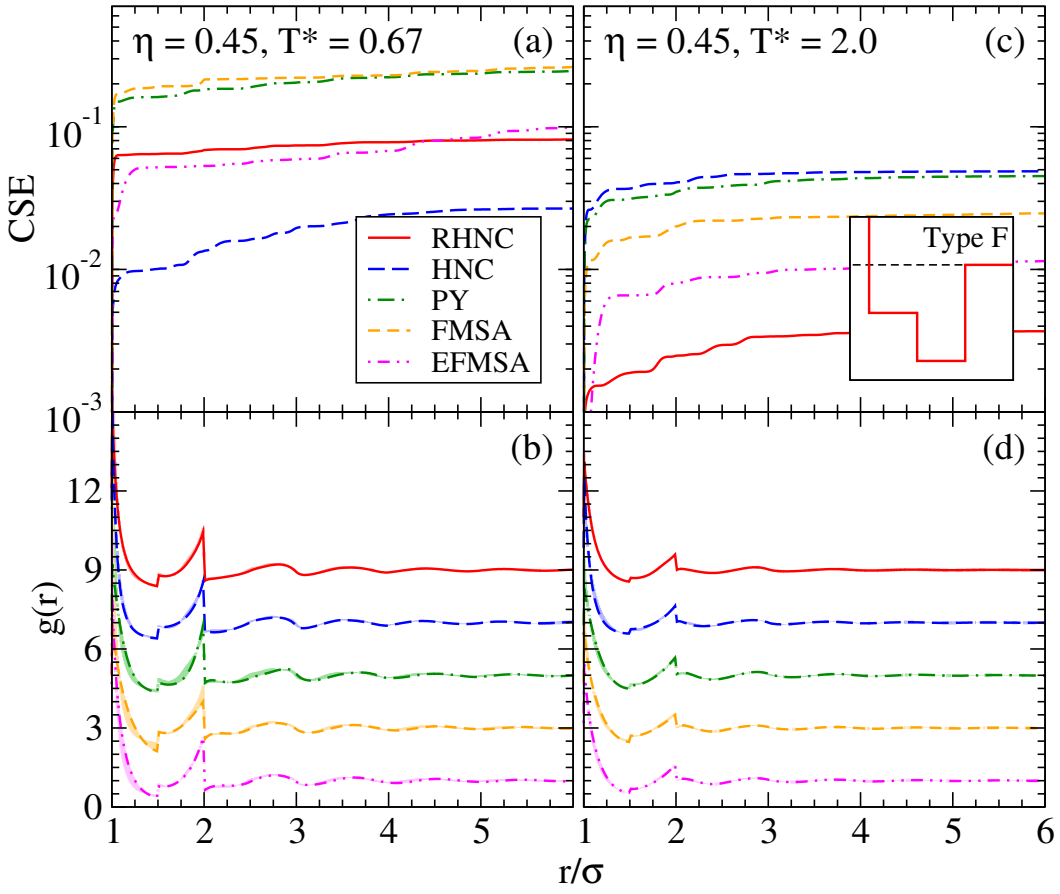

Figure B.5: Radial distribution functions and cumulative squared errors for the "Type F" pair interaction. Series are as in Fig. B.1.

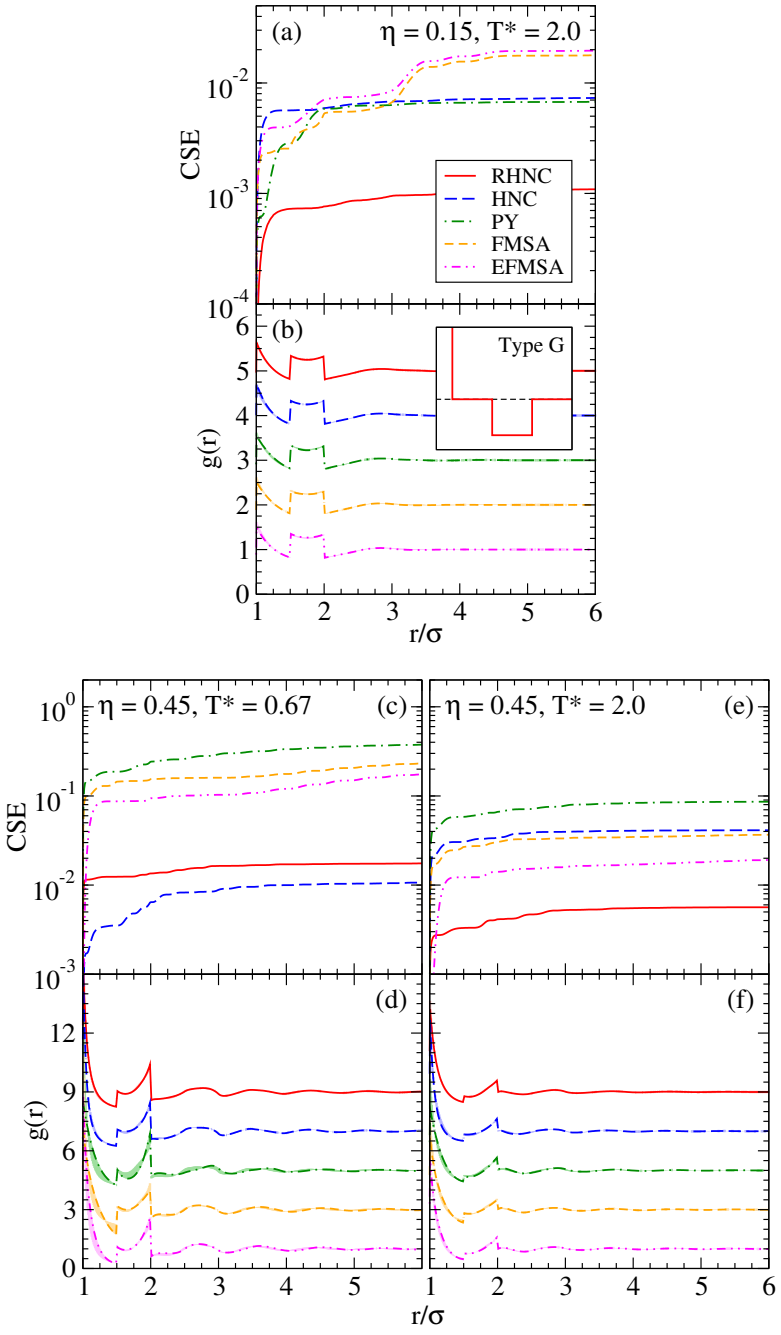

Figure B.6: Radial distribution functions and cumulative squared errors for the "Type G" pair interaction. Series are as in Fig. B.1.

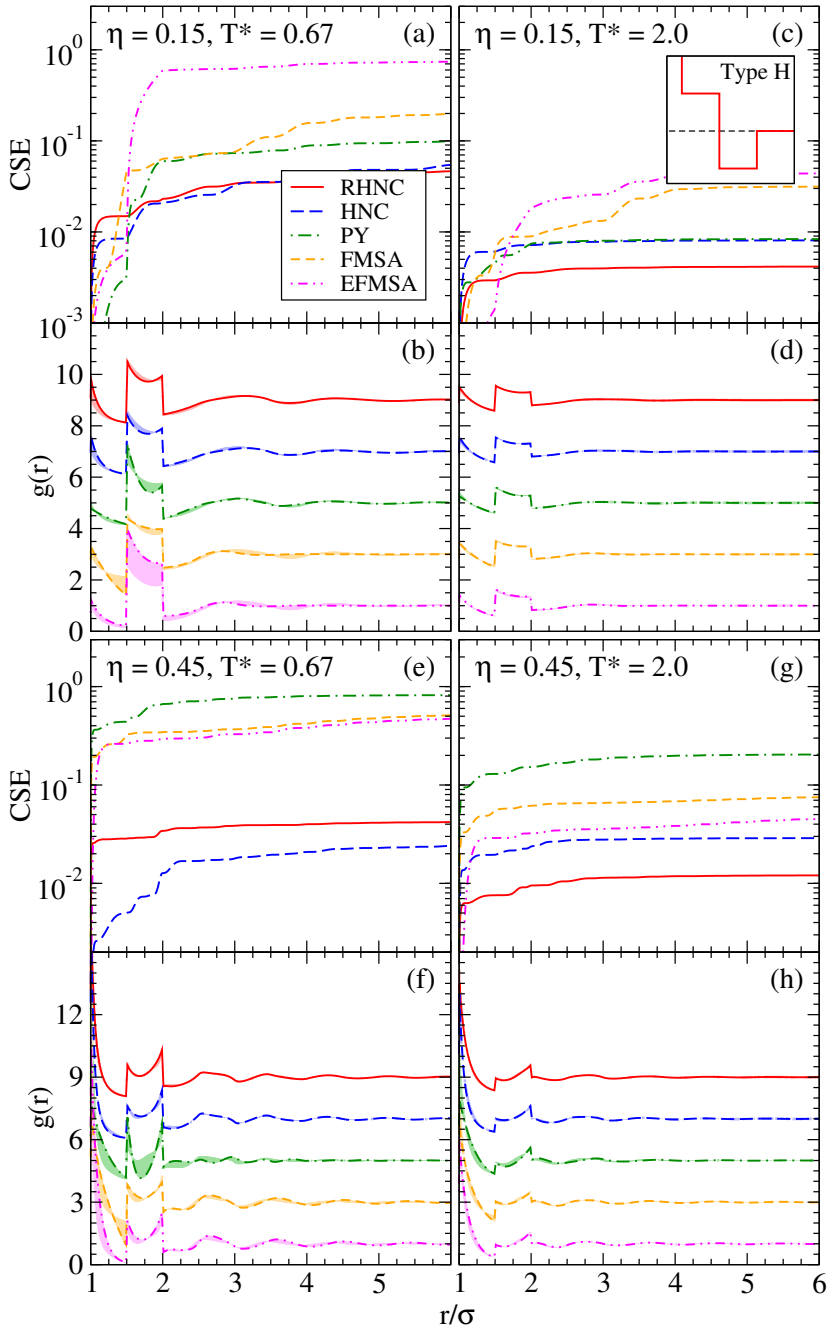

Figure B.7: Radial distribution functions and cumulative squared errors for the "Type H" pair interaction. Series are as in Fig. B.1.

Appendix C

Complete Thermodynamic Error Tables

The absolute normalized potential energy error, $|(U_{\text{thy}}/U_{\text{sim}}) - 1|$, and the absolute normalized two-body excess etntropy error, $\left|\left(s^{(2)}_{\text{thy}}/s^{(2)}_{\text{sim}}\right) - 1\right|$, are tabulated in Table C.1 and Table C.2, respectively.

Table C.1: Absolute normalized potential energy error, $|(U_{\text{thy}}/U_{\text{sim}}) - 1|$, for all approaches, state points, and interactions considered. The labels "R," "H," and "P" are the RHNC [31, 47], HNC [31], and PY [31] closures to the Ornstein-Zernike relation, respectively. "F" is the FMSA [65], and "E" is the EFMSA [36]. Italics indicate the value closest to zero (e.g., a perfect prediction) at each combination of state point and interaction type.

	Type A				Type B			
T^*	0.67		2.00		0.67		2.00	
η	0.15	0.45	0.15	0.45	0.15	0.45	0.15	0.45
R	*0.000*	0.003	*0.000*	*0.000*	0.007	0.021	*0.001*	0.007
H	0.000	0.002	0.001	0.000	*0.005*	0.028	0.001	0.021
P	0.019	0.006	0.007	0.006	0.006	0.019	0.002	*0.008*
F	0.097	*0.001*	0.015	0.002	0.182	*0.008*	0.018	0.012
E	0.079	0.008	0.019	0.003	0.091	0.043	0.012	0.005

	Type C				Type D			
T^*	0.67		2.00		0.67		2.00	
η	0.15	0.45	0.15	0.45	0.15	0.45	0.15	0.45
R	0.025	0.038	0.004	0.014	0.140	*0.113*	0.110	0.613
H	0.022	0.048	*0.001*	0.040	*0.135*	0.119	0.078	1.698
P	*0.002*	*0.028*	0.005	*0.007*	0.189	0.250	0.080	2.030
F	0.501	0.036	0.020	0.015	0.181	0.610	*0.040*	*0.520*
E	0.245	0.143	0.034	0.035	0.472	0.146	0.072	3.431

	Type E				Type F			
T^*	0.67		2.00		0.67		2.00	
η	0.15	0.45	0.15	0.45	0.15	0.45	0.15	0.45
R	–[a]	–[a]	–[a]	0.002	–[a]	0.061	–[a]	0.006
H	–[a]	–[a]	–[a]	*0.000*	–[a]	0.039	–[a]	0.015
P	–[a]	–[a]	–[a]	0.003	–[a]	0.084	–[a]	0.011
F	–[a]	–[a]	–[a]	0.005	–[a]	0.094	–[a]	0.020
E	–[a]	–[a]	–[a]	0.000	–[a]	*0.013*	–[a]	*0.003*

	Type G				Type H			
T^*	0.67		2.00		0.67		2.00	
η	0.15	0.45	0.15	0.45	0.15	0.45	0.15	0.45
R	–[a]	*0.005*	*0.001*	*0.010*	*0.073*	*0.079*	0.021	0.041
H	–[a]	0.016	0.002	0.025	0.086	0.129	0.026	0.075
P	–[a]	0.096	0.014	0.042	0.103	0.387	0.016	0.289
F	–[a]	0.026	0.013	0.023	0.140	0.200	*0.015*	*0.029*
E	–[a]	0.051	0.015	0.017	0.536	0.110	0.051	0.221

[a] Simulated system is not a single-phase, uniform fluid at equilibrium.

Table C.2: Absolute normalized 2-body excess entropy error, $|(s^{(2)}_{\text{thy}}/s^{(2)}_{\text{sim}}) - 1|$, for all approaches, state points, and interactions considered. Labels are as in Table C.1. Italics indicate the value closest to zero (e.g., a perfect prediction) at each combination of state point and interaction type.

	Type A				Type B			
T^*	0.67		2.00		0.67		2.00	
η	0.15	0.45	0.15	0.45	0.15	0.45	0.15	0.45
R	*0.003*	*0.004*	*0.002*	*0.002*	0.018	0.047	0.004	0.004
H	0.010	0.008	0.009	0.022	0.014	0.073	*0.003*	0.015
P	0.024	0.005	0.020	0.005	0.021	0.106	0.022	*0.000*
F	0.010	0.006	0.005	0.006	0.320	0.048	0.009	0.012
E	0.032	0.011	0.012	0.004	*0.012*	*0.022*	0.010	0.047

	Type C				Type D			
T^*	0.67		2.00		0.67		2.00	
η	0.15	0.45	0.15	0.45	0.15	0.45	0.15	0.45
R	0.026	*0.019*	0.007	0.008	0.215	0.176	0.024	*0.010*
H	0.024	0.045	*0.000*	0.025	0.211	*0.161*	0.018	0.034
P	*0.018*	0.098	0.013	0.016	0.255	0.287	0.019	0.052
F	0.469	0.054	0.014	*0.006*	*0.161*	0.456	*0.008*	0.031
E	0.152	0.042	0.005	0.062	0.387	0.463	0.040	0.076

	Type E				Type F			
T^*	0.67		2.00		0.67		2.00	
η	0.15	0.45	0.15	0.45	0.15	0.45	0.15	0.45
R	–[a]	–[a]	–[a]	0.013	–[a]	0.176	–[a]	0.036
H	–[a]	–[a]	–[a]	0.021	–[a]	0.073	–[a]	0.036
P	–[a]	–[a]	–[a]	0.046	–[a]	0.117	–[a]	*0.022*
F	–[a]	–[a]	–[a]	*0.007*	–[a]	0.239	–[a]	0.045
E	–[a]	–[a]	–[a]	0.004	–[a]	*0.032*	–[a]	0.034

	Type G				Type H			
T^*	0.67		2.00		0.67		2.00	
η	0.15	0.45	0.15	0.45	0.15	0.45	0.15	0.45
R	–[a]	0.051	0.003	0.040	0.185	*0.068*	0.012	0.057
H	–[a]	0.032	0.011	0.041	0.192	0.170	*0.011*	0.039
P	–[a]	0.138	0.020	*0.024*	0.219	0.161	0.020	0.136
F	–[a]	*0.025*	0.021	0.036	*0.023*	0.181	0.014	*0.001*
E	–[a]	0.181	*0.001*	0.049	0.533	0.531	0.027	0.066

[a] Simulated system is not a single-phase, uniform fluid at equilibrium.

Bibliography

[1] Evan H. Abramson. Viscosity of water measured to pressures of 6 GPa and temperatures of 300 °C. *Physical Review E*, 76:051203, 2007.

[2] Evan H. Abramson. Viscosity of carbon dioxide measured to a pressure of 8 GPa and temperature of 673 K. *Physical Review E*, 80:021201, 2009.

[3] Evan H. Abramson and Hoku West-Foyle. Viscosity of nitrogen measured to pressures of 7 GPa and temperatures of 573 K. *Physical Review E*, 77:041202, 2008.

[4] Manish Agarwal, Murari Singh, B. Shadrack Jabes, and Charusita Chakravarty. Excess entropy scaling of transport properties in network-forming ionic melts (SiO_2 and BeF_2). *The Journal of Chemical Physics*, 134(1):014502, 2011.

[5] Michael P. Allen and Dominic J. Tildesley. *Computer Simulation of Liquids*. Oxford Science Publ. Clarendon Press, 1989.

[6] Hans C. Andersen. Molecular dynamics simulations at constant pressure and/or temperature. *The Journal of Chemical Physics*, 72(4):2384–2393, 1980.

[7] Jacob Andkjær, Villads Egede Johansen, Kasper Storgaard Friis, and Ole Sigmund. Inverse design of nanostructured surfaces for color effects. *Journal of the Optical Society of America B*, 31(1):164–174, 2014.

[8] Sho Asakura and Fumio Oosawa. Interaction between particles suspended in solutions of macromolecules. *Journal of Polymer Science*, 33(126):183–192, 1958.

[9] Marcus N. Bannerman and Leo Lue. Exact on-event expressions for discrete potential systems. *The Journal of Chemical Physics*, 133(12):124506, 2010.

[10] Marcus N. Bannerman, Robert Sargant, and Leo Lue. DynamO: A free $\mathcal{O}(N)$ general event-driven molecular dynamics simulator. *Journal of Computational Chemistry*, 32(15):3329–3338, 2011.

[11] Ana Laura Benavides and Alejandro Gil-Villegas. The thermodynamics of molecules with discrete potentials. *Molecular Physics*, 97(12):1225–1232, 1999.

[12] Jonathan A. Bollinger, Avni Jain, and Thomas M. Truskett. Structure, thermodynamics, and position-dependent diffusivity in fluids with sinusoidal density variations. *Langmuir*, 30(28):8247–8252, 2014.

[13] Andy Buffler, Seshini Pillay, Fred Lubben, and Roger Fearick. A model-based view of physics for computational activities in the introductory physics course. *American Journal of Physics*, 76(4):431–437, 2008.

[14] James Carmer, Gaurav Goel, Mark J. Pond, Jeffrey R. Errington, and Thomas M. Truskett. Enhancing tracer diffusivity by tuning interparticle interactions and coordination shell structure. *Soft Matter*, 8:4083–4089, 2012.

[15] James Carmer, Gaurav Goel, Mark J. Pond, Jeffrey R. Errington, and Thomas M. Truskett. Enhancing tracer diffusivity by tuning interparticle interactions and coordination shell structure. *Soft Matter*, 8:4083–4089, 2012.

[16] Janet M. Casperson and Marcia C. Linn. Using visualizations to teach electrostatics. *American Journal of Physics*, 74(4):316–323, 2006.

[17] Qian Chen, Sung Chul Bae, and Steve Granick. Directed self-assembly of a colloidal Kagome lattice. *Nature*, 469:381–384, 2011.

[18] Ravi Chopra, Thomas M. Truskett, and Jeffrey R. Errington. Excess entropy scaling of dynamic quantities for fluids of dumbbell-shaped particles. *The Journal of Chemical Physics*, 133(10):104506, 2010.

[19] T. W. Cochran and Yee C. Chiew. Thermodynamic and structural properties of repulsive hard-core Yukawa fluid: Integral equation theory, perturbation theory and Monte Carlo simulations. *The Journal of Chemical Physics*, 121(3):1480–1486, 2004.

[20] Henry Cohn and Abhinav Kumar. Algorithmic design of self-assembling structures. *Proceedings of the National Acadademy of Sciences of the United States of America*, 106(24):9570–9575, 2009.

[21] Bahman Davoudi, Mohammad Kohandel, M. Mohammadi, and Bilal Tanatar. Hard-core Yukawa model for charge-stabilized colloids. *Physical Review E*, 62:6977–6981, 2000.

[22] Mikhail Dzugutov. A universal scaling law for atomic diffusion in condensed matter. *Nature*, 381:137–139, 1996.

[23] Erik Edlund, Oskar Lindgren, and Martin Nilsson Jacobi. Designing isotropic interactions for self-assembly of complex lattices. *Physical Review Letters*, 107:085503, 2011.

[24] Jeffrey R. Errington, Thomas M. Truskett, and Jeetain Mittal. Excess-entropy-based anomalies for a waterlike fluid. *The Journal of Chemical Physics*, 125(24):244502, 2006.

[25] Étienne Marcotte, Frank H. Stillinger, and Sal Torquato. Unusual ground states via monotonic convex pair potentials. *The Journal of Chemical Physics*, 134(16):164105, 2011.

[26] Étienne Marcotte, Frank H. Stillinger, and Salvatore Torquato. Communication: Designed diamond ground state via optimized isotropic monotonic pair potentials. *The Journal of Chemical Physics*, 138(6):061101, 2013.

[27] Sharon C Glotzer and Michael J. Solomon. Anisotropy of building blocks and their assembly into complex structures. *Nature Materials*, 6:557–562, 2007.

[28] Nicoletta Gnan, Thomas B. Schrøder, Ulf R. Pedersen, Nicholas P. Bailey, and Jeppe C. Dyre. Pressure-energy correlations in liquids. IV. Isomorphs in liquid phase diagrams. *The Journal of Chemical Physics*, 131(23):234504, 2009.

[29] Gaurav Goel, William P. Krekelberg, Jeffrey R. Errington, and Thomas M. Truskett. Tuning density profiles and mobility of inhomogeneous fluids. *Physical Review Letters*, 100:106001, 2008.

[30] Gaurav Goel, William P Krekelberg, Mark J Pond, Jeetain Mittal, Vincent K Shen, Jeffrey R Errington, and Thomas M Truskett. Available states and available space: Static properties that predict self-diffusivity of confined fluids. *Journal of Statistical Mechanics: Theory and Experiment*, 2009(04):P04006, 2009.

[31] Jean-Pierre Hansen and Ian R. McDonald. *Theory of Simple Liquids*. Elsevier Science, 2006.

[32] Jean-Pierre Hansen and Loup Verlet. Phase transitions of the Lennard-Jones system. *Physical Review*, 184:151–161, 1969.

[33] Marco Heinen, Peter Holmqvist, Adolfo J. Banchio, and Gerhard Nägele. Pair structure of the hard-sphere Yukawa fluid: An improved analytic

method versus simulations, Rogers-Young scheme, and experiment. *The Journal of Chemical Physics*, 134(4):044532, 2011.

[34] Douglas Henderson and E. W. Grundke. Direct correlation function: Hard sphere fluid. *The Journal of Chemical Physics*, 63(2):601–607, 1975.

[35] R.L. Henderson. A uniqueness theorem for fluid pair correlation functions. *Physics Letters A*, 49(3):197–198, 1974.

[36] Stepan P. Hlushak, P. A. Hlushak, and Andrij D. Trokhymchuk. An improved first-order mean spherical approximation theory for the square-shoulder fluid. *The Journal of Chemical Physics*, 138(16):164107, 2013.

[37] Stepan P. Hlushak, Andrij D. Trokhymchuk, and Stefan Sokolowski. Direct correlation function for complex square barrier-square well potentials in the first-order mean spherical approximation. *The Journal of Chemical Physics*, 134(11):114101, 2011.

[38] G. Hummer, S. Garde, A. E. Garca, M. E. Paulaitis, and L. R. Pratt. Hydrophobic effects on a molecular scale. *Journal of Physical Chemistry B*, 102(51):10469–10482, 1998.

[39] E. A. Jagla. Core-softened potentials and the anomalous properties of water. *The Journal of Chemical Physics*, 111(19):8980–8986, 1999.

[40] Avni Jain, Jonathan A. Bollinger, and Thomas M. Truskett. Inverse methods for material design. *AIChE Journal*, 60(8):2732–2740, 2014.

[41] Avni Jain, Jeffrey R. Errington, and Thomas M. Truskett. Inverse design of simple pairwise interactions with low-coordinated 3D lattice ground states. *Soft Matter*, 9:3866–3870, 2013.

[42] William P. Krekelberg, Jeetain Mittal, Venkat Ganesan, and Thomas M. Truskett. How short-range attractions impact the structural order, self-diffusivity, and viscosity of a fluid. *The Journal of Chemical Physics*, 127(4):044502, 2007.

[43] William P Krekelberg, Mark J Pond, Gaurav Goel, Vincent K Shen, Jeffrey R Errington, and Thomas M Truskett. Generalized Rosenfeld scalings for tracer diffusivities in not-so-simple fluids: Mixtures and soft particles. *Physical Review E*, 80(6):061205, 2009.

[44] Stanislav Labík, Anatol Malijevský, and Petr Voňka. A rapidly convergent method of solving the OZ equation. *Molecular Physics*, 56(3):709–715, 1985.

[45] James Laverty and Gerd Kortemeyer. Function plot response: A scalable system for teaching kinematics graphs. *American Journal of Physics*, 80(8):724–733, 2012.

[46] Christos N. Likos. Effective interactions in soft condensed matter physics. *Physics Reports*, 348(45):267–439, 2001.

[47] Anatol Malijevský and Stanislav Labík. The bridge function for hard spheres. *Molecular Physics*, 60(3):663–669, 1987.

[48] Jeetain Mittal, Thomas M. Truskett, Jeffrey R. Errington, and Gerhard Hummer. Layering and position-dependent diffusive dynamics of confined fluids. *Physical Review Letters*, 100:145901, 2008.

[49] Ángel Mulero, Francisco Cuadros, and M. Pérez-Ayala. Displaying the role of repulsive and attractive intermolecular forces in fluids. *American Journal of Physics*, 61(7), 1993.

[50] R. E. Nettleton and M. S. Green. Expression in terms of molecular distribution functions for the entropy density in an infinite system. *The Journal of Chemical Physics*, 29(6), 1958.

[51] Mark J Pond, Jeffrey R Errington, and Thomas M Truskett. Communication: Generalizing Rosenfeld's excess-entropy scaling to predict long-time diffusivity in dense fluids of brownian particles: From hard to ultrasoft interactions. *The Journal of Chemical Physics*, 134(8):081101, 2011.

[52] Mark J. Pond, William P. Krekelberg, Vincent K. Shen, Jeffrey R. Errington, and Thomas M. Truskett. Composition and concentration anomalies for structure and dynamics of Gaussian-core mixtures. *The Journal of Chemical Physics*, 131(16):161101, 2009.

[53] Dennis C. Rapaport. *The Art of Molecular Dynamics Simulation*. Cambridge University Press, 2004.

[54] David R Reichman and Patrick Charbonneau. Mode-coupling theory. *Journal of Statistical Mechanics: Theory and Experiment*, 2005(05):P05013, 2005.

[55] Forrest J. Rogers and David A. Young. New, thermodynamically consistent, integral equation for simple fluids. *Physical Review A*, 30:999–1007, 1984.

[56] Yaakov Rosenfeld. Relation between the transport coefficients and the internal entropy of simple systems. *Physical Review A*, 15:2545–2549, 1977.

[57] Yaakov Rosenfeld. A quasi-universal scaling law for atomic transport in simple fluids. *Journal of Physics: Condensed Matter*, 11(28):5415, 1999.

[58] Roland Roth, Robert Evans, and Sigfried Dietrich. Depletion potential in hard-sphere mixtures: theory and applications. *Physical Review E*, 62:5360–5377, 2000.

[59] Andrés Santos, Santos Bravo Yuste, Mariano López de Haro, Mariana Bárcenas, and Pedro Orea. Structural properties of fluids interacting via piece-wise constant potentials with a hard core. *The Journal of Chemical Physics*, 139(7):074505, 2013.

[60] Ruchi Sharma, Somendra Nath Chakraborty, and Charusita Chakravarty. Entropy, diffusivity, and structural order in liquids with waterlike anomalies. *The Journal of Chemical Physics*, 125(20):204501, 2006.

[61] William R. Smith, Douglas Henderson, and John A. Barker. Perturbation theory and the radial distribution function of the squarewell fluid. *The Journal of Chemical Physics*, 55(8):4027–4033, 1971.

[62] José Ramón Solana. Thermodynamic properties of double square-well fluids: Computer simulations and theory. *The Journal of Chemical Physics*, 129(24):244502, 2008.

[63] Frank H. Stillinger, Salvatore Torquato, Juan M. Eroles, and Thomas M. Truskett. Iso-$g^{(2)}$ processes in equilibrium statistical mechanics. 105(28):6592–6597, 2001.

[64] Yiping Tang. On the first-order mean spherical approximation. *The Journal of Chemical Physics*, 118(9):4140–4148, 2003.

[65] Yiping Tang and Benjamin C.-Y. Lu. Analytical representation of the radial distribution function for classical fluids. *Molecular Physics*, 90(2):215–224, 1997.

[66] Jan Tobochnik and Harvey Gould. Teaching statistical physics by thinking about models and algorithms. *American Journal of Physics*, 76(4):353–359, 2008.

[67] Salvatore Torquato. Inverse optimization techniques for targeted self-assembly. *Soft Matter*, 5:1157–1173, 2009.

[68] Loup Verlet and Jean-Jacques Weis. Equilibrium theory of simple liquids. *Physical Review A*, 5:939–952, 1972.

[69] Carl E. Wieman, Katherine K. Perkins, and Wendy K. Adams. Oersted Medal Lecture 2007: Interactive simulations for teaching physics: What works, what doesn't, and why. *American Journal of Physics*, 76(4):393–399, 2008.

[70] Limei Xu, Sergey V. Buldyrev, C. Austen Angell, and H. Eugene Stanley. Thermodynamics and dynamics of the two-scale spherically symmetric Jagla ramp model of anomalous liquids. *Physical Review E*, 74:031108, 2006.

[71] Zhenyu Yan, Sergey V. Buldyrev, Nicolas Giovambattista, Pablo G. Debenedetti, and H. Eugene Stanley. Family of tunable spherically symmetric potentials that span the range from hard spheres to waterlike behavior. *Physical Review E*, 73:051204, 2006.

[72] Anand Yethiraj and Alfons van Blaaderen. A colloidal model system with an interaction tunable from hard sphere to soft and dipolar. *Nature*, 421(6922):513, 2003.

[73] K. Younge, C. Christenson, A. Bohara, J. Crnkovic, and P. Saulnier. A model system for examining the radial distribution function. *American Journal of Physics*, 72(9):1247, 2004.

[74] Santos Bravo Yuste, Andrés Santos, and Mariano López de Haro. Structure of the square-shoulder fluid. *Molecular Physics*, 109(6):987–995, 2011.

[75] Gilles Zerah and Jean-Pierre Hansen. Self-consistent integral equations for fluid pair distribution functions: Another attempt. *The Journal of Chemical Physics*, 84(4):2336–2343, 1986.

[76] Shiqi Zhou. Thermodynamic perturbation theory in fluid statistical mechanics. *Physical Review E*, 74:031119, 2006.

[77] Shiqi Zhou. Fifth-order thermodynamic perturbation theory of uniform and nonuniform fluids. *Physical Review E*, 77:041110, 2008.